2021 Annual Report

Institute of Biophysics

Department of Nanobiotechnology

University of Natural Resources and Life Sciences

Vienna, Austria

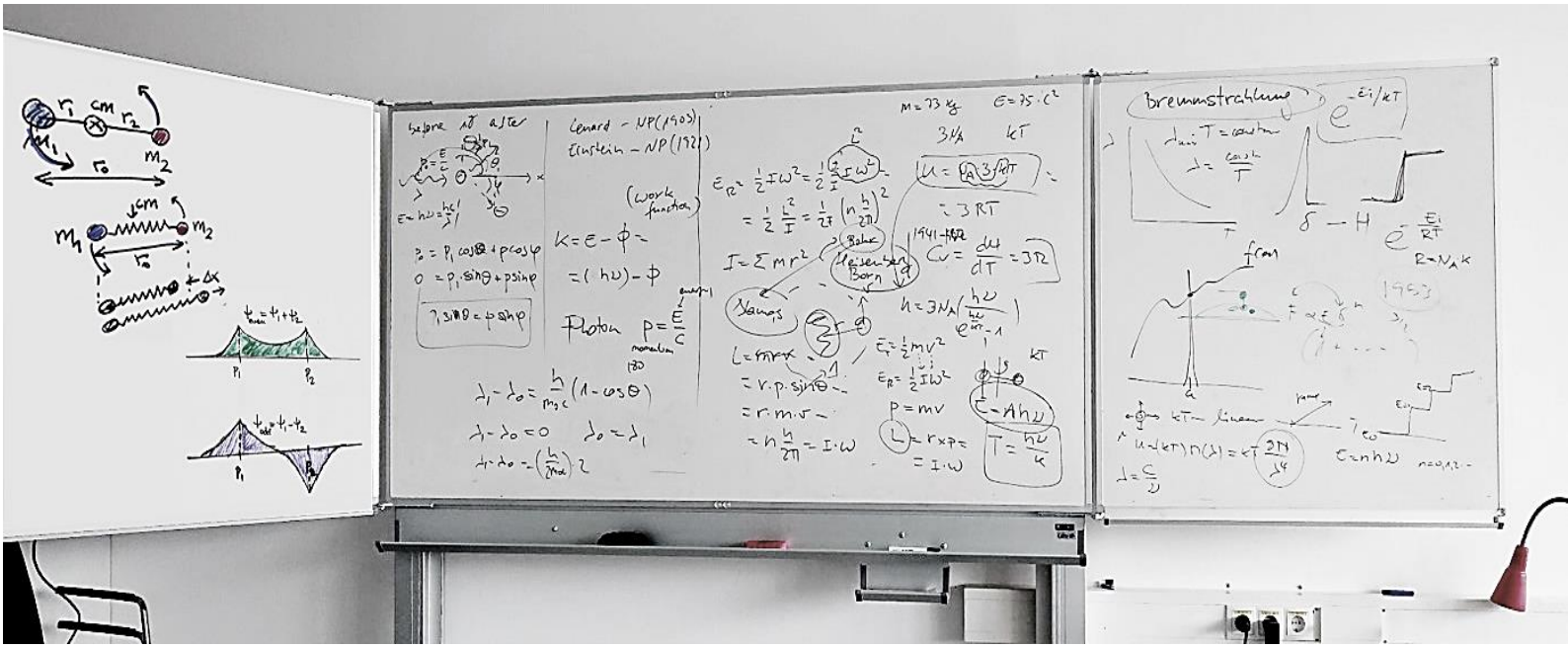

2021 Annual Report
Institute of Biophysics

Department of Nanobiotechnology
University of Natural Resources and Life Sciences, Austria

Foreword

2021. Second Bi-annual report that we still call “annual report”. The highlight of the year was the international evaluation of the department (and the institute). We were evaluated by external referees as “excellent” although it is unclear which consequences (for good or bad) this will have. Anyway, I am happy and proud of you all but also tired (of the administration and its subtle tensile force). That is why I proposed to Erik Reimhult and Eva Ehmoser to elect another head of department for the next three years.

2021 was also the second Covid-19 year (with all the consequences for our health, teaching, and research activities). Here, I must express my gratitude to all of you who made my (administrative) work easy. I should not forget, the people who maintained the laboratories of the institute (and department) alive. As usual we had BOKU and DNBT duties to fulfill. We have had “external” researches in our labs during this strange times. Teaching on-line has become a tool that will be important in the years to come (hybrid lectures, seminars, groups meeting, conferences, etc. will be using this technology). As a matter of routine, we participated in commissions and working groups concerning leadership, teaching, research and ethical matters (DLK, DokStuko, FachStuko, Forschungsprecher, ethics platform, habilitation group). No more comments about that.

The institute had a good year. Some students (Andi, Dmitri, Ewa, Lukas, Martin, Nora, Theresa) got their and PhD and MSc degrees. Notburga has closed successfully his ERC project with a large number of publications, which contributed to the visibility of the institute. Furthermore, we have published about 28 articles as main or supportive authors (and we got some cover pictures as well). In addition, we all have presented our results in about 20 conferences, workshops or invited talks.

Following the “international” and “open doors” tradition of our institute, we hosted this year 4 visiting scientist from professor to student level. A highlight was to have Antonio Lucas (University of Zaragoza) as a BOKU visiting professor. This expanded our

boundaries to translational research since Antonio (who teaches psychology) explained in his lecture how traffic and its derived problems can be conceptualized with physics (distance, speed, flow equations, waves and chaos). Another highlight was the visit of Cristina Satriano (University of Catania) who visited the department (BiMAT) within the Erasmus program to teach Biomaterials and Biointerface science, and also did some measurements with us.

2022 will be a nice challenge.

We will have a generational change. Dietmar Pum will retire after 40 years at BOKU (which means that S-layer research will no longer be an active line of research), Jagoba and Juan Carlos will also leave (to pursue their careers) and most of the master's and PhD students will have finished. In fact, Jagoba has found a position in CIDETEC (Spain) that represents a step forward in his career, which follows the successful trend of the alumni of the institute.

This would imply a restructuring of the institute with new assistants and students. We may have to reorganize Dietmar's teaching in optics-related courses (if we get the right support from the rectorate). In this context, our teaching will continue to be dedicated to MSc and PhD students. We still need a compulsory teaching at bachelor level to introduce our future students to the necessary basic knowledge in biological physics. This is my wish, but it will not happen.... Nevertheless, we should be happy.

Overall, our research is in good shape. We have developed new topics ranging from the molecular to the macroscopic and we may need to obtain some grants to maintain the level of work we have achieved. We should deepen the understanding and application of our experimental techniques. We should not forget theory and computational support (i.e. machine learning). Cooperation with other BOKU departments might give our research (and teaching) an inter- and transdisciplinary touch.

During 2021, we have been 25 people between members and visitors. Among them: 5 PhD students, 3 MSc students. They are the future.

I thank everybody who have made this report possible. As always, I wish all the best to the coworkers who have left the Institute to continue their careers elsewhere.

Thank you.

José L. Toca-Herrera

Contents

Institute members and visitors

Research projects

- S-layer protein and carbon nanotube construction kit
- Hard plant shells: How cell walls determine tissue mechanics
- Nutshell structures for high strength and energy absorption
- Bacterial cellulose: kombucha production blended with walnut shells
- Walnut cells cellulosic walls and their role in 3D puzzle cells morphogenesis
- Raman imaging of Micrasterias: new insights into shape formation
- A guide to hidden multicomponent layered structure of plant cuticles
- Raman imaging reveals microchemistry of spruce needles
- Oak wood drying: precipitation of ellagic acid leads to discoloration
- Larch species and their hybrid: different responses to drought stress
- Major components of hyalinosis in the arteriolosclerotic ulcer of Martorell
- Cell stiffness: effects of actin disruptors CK-869 and jasplakinolide
- Nucleotides-Induced Changes in Living Endothelial Cells and Astrocytes
- Stimulation/blocking of receptor P2X7: response of cerebellar astrocytes
- Human Colorectal Cancer Cells: Time- and Zinc-Related Changes
- Alginate-based aerogels: mech. properties upon buffer-dependent swelling
- Electrospun poly-urethane vascular grafts: mech. behavior and degradation
- Neural stem cells: nanostructured scaffolds based on bioresorbable polymers graphene
- Sox2 Cell Adhesion in MCF7 Breast Cancer Cells
- MCF7 and HEK-293 cells: early-stage cell-cell and cell-substrate adhesion
- Enhanced cell attachment through hierarchical Polymer-based niches
- Effects of substrate elasticity on the viscoelastic properties of MCF-7 cells
- Titin 27: mech. unfolding through temperature and hydrophobic forces
- Titin I27: Expression and characterization of mechanical unfolding with AFM
- Expression of Titin I27 polyprotein and its mutants
- FLNA editing regulates cellular adhesion, migration and mech. properties
- Machine Learning Approaches to Classify AFM Force Spectroscopy Curves
- Automatic Detection of Protein Unfolding Events in AFM studies
- Automatic Detection of Tethers and other Adhesions in Retraction Curves
- Viscoelastic Properties of Eukaryotic Cells Measured with AFM
- Modelling cell fluidisation after actin depolymerisation using AFM
- Can we use power laws to describe the mechanical properties of bacteria?
- Viscoelasticity of bacterial cells measured by AFM creep experiments
- Power laws in eukaryotic cell mechanics based on AFM measurements
- Frequency dependence of mech. properties of different biological materials
- Estrogen on Epithelial Breast Cancer Cell Mechanics & Cell-to-Cell Contacts
- Estrogen receptor on drugs and mech. properties of epithelial breast cancer cells
- New tricks for an old dog: Including afmmulti in the R afmToolkit

Publications

Conferences, seminars, schools and workshops

Ongoing projects, national and international collaborations

1. Institute members and visitors - 2021

Univ. Prof. Dr. José L. Toca-Herrera (director)
Ao. Univ. Prof. Dr. Dietmar Pum (deputy director)
Assoc. Prof. Dr. Notburga Gierlinger (group leader)
Assoc. Prof. Antonio Lucas Alba (BOKU – guest professor, University of Zaragoza)
Assoc. Prof. Dr. Luis Millan Gonzalez (University of Valencia)
Assoc. Prof. Maria Teresa Pellicer (University of Valencia)
Assoc. Prof. Cristina Satriano (University of Catania)
Dr. Peter Bock (postdoc)
Dr. Andreas Breitwieser (postdoc)
Dr. Martin Feldhofer (postdoc)
Dr. Jessica Huss (postdoc)
Dr. Jagoba Iturri (senior scientist)
Dr. Juan Carlos Gil-Redondo (univ. assistant)
Dr. Andreas Weber (PhD student and postdoc)
Mag. Amsatou Andorfer-Sarr (techn. assistant)
Mag. Jacqueline Friedmann (tech. assistant)
MSc Sebastian Antreich (PhD student)
Dr. Med. Michael Handler (PhD student, collaboration with Sports University of Innsbruck)
MSc. Nadia Sasani (PhD student)
MSc. Nannan Xiao (PhD student)
BSc Ulrich Fuchs (MSc Student)
BSc Lukas Krismer (MSc student)
BSc Dmitri Morozov (MSc student, collaboration TU-Wien)
Hannah Blaschka (apprentice)
Walter Klug (IT technician)

2. Research projects

S-layer protein and carbon nanotube construction kit

Dietmar Pum[1], *Andreas Breitwieser*[1]

[1]Institute of Biophysics, Department of Nanobiotechnology, University of Natural Resources and Life Science, Vienna, Austria

Objective

The main goal of the project was to study the reassembly of wild type and genetically functionalized S-layer fusion proteins on the surface of multi walled carbon nanotubes (MWNTs) and to learn how these composites can be used to fabricate new organic-inorganic hybrid materials.

Results & Conclusion

S-layer proteins form the outermost cell envelope component in a wide range of bacteria and archaea. [1,2] They can be considered as one of the most abundant biopolymers on earth. Identical onto the surface of bacterial cells, S-layer proteins have the natural ability to reassemble into crystalline monomolecular arrays on solid supports, at the air-water interface, on planar lipid films, and liposomes.

The successful coating of the wild-type wtSbpA S-layer protein from *Lysinibacillus stearothermohilus* CCM2177 and the recombinant fusion protein rSbpA$_{31-1068}$GG (consisting of the reassembling part of the S-layer protein and two copies of the IgG binding region of Protein G) on multi walled carbon nanotubes (MWNTs) laid foundation for the success of the project (reported 2019). [3] In a subsequent optimization step, the protocol for S-layer reassembly could be modified such that even pristine MWNTs (without surface modification) could be dispersed (zeta potential: -24.4 +/- 0.6 mV @ pH 7) and subsequently completely covered by S-layer proteins. [4] Moreover, the developed new preparation protocol was also successfully applied for the recrystallization of wtSbpA S-layer protein on graphene sheets. [4]

After these important reassembly experiments, we successfully extended our S-layer protein portfolio with SbsB, the S-layer protein from *Geobacillus stearothermophilus* PV72/p2, and the S-layer proteins type I L111 and type III S102 from *Th. thermohydrosulfuricum*. While SbsB forms regular arrays with oblique (p1) lattice symmetry, type I L111 and type III S102 lead to lattices with hexagonal (p6) lattice symmetry. However, while work with SbsB always resulted in highly ordered, clearly visible lattices on the MWNT surfaces, the tubes coated with type I L111 and type III S102 showed only weak contrast in TEM images and often no complete coverage.

In addition, reassembly experiments where a mixture of both S-layer proteins (SbpA and SbsB) was offered to a solution of pristine MWNTs were carried out too. [4] It is interesting to see that the carbon nanotubes are covered by SbsB with its oblique lattice symmetry, while SbpA forms only self-assembly products with square lattice symmetry in the background. We suggest that the competition in forming a crystalline monolayer on the MWNT surface is favored by the simpler oblique lattice symmetry of SbsB compared to the square lattice symmetry of SbpA. In the course of a further optimization step of the S-layer

coating conditions, it was found that SbpA is also able to follow the curved hemispherical caps of closed nanotubes. [4]

Reassembly experiments were performed with the S-layer fusion protein rSbpA Strep-tag II on pristine MWNTs to align the carbon nanotubes into parallel bundles. Although proof in principle was obtained after incubation with streptavidin as linker molecules, elongated parallel bundles could not be observed because the nanotubes were not straight even over longer distances.

Once we had established this S-layer technology base, we began to explore the use of S-layer coated MWNTs as scaffolds in biomineralization processes. Based on our findings, we investigated the precipitation of gold from chloroauric acid solutions ($HAuCl_4$) on wtSbpA S-layer proteins and, alternatively, the binding of preformed Au(Ni) nanoparticles on rSbpA-His tag fusion proteins. In all approaches (including chemical modification of the S-layer protein with iminothiolane (IT) / dithiothreitol (DTT)) gold was selectively deposited on the S-layer (often) in a very dense packing, but a highly ordered arrangement of the nanoparticles was nevertheless never found.

Based on previous experiments with S-layer coated liposomes, MWNTs were silicified with tetramethoxysilane (TMOS) in a mild biogenic approach in order to obtain a chemically inert glass-like coating on the nanotube surface. As expected, the thickness of the silica layer could be controlled by the reaction time and was 6.3 +/- 1.25 nm after 5 min and 25.0 +/- 5.9 nm after 15 min. It is worth noting that the thickness of the silica layer after 5 min of silicification time is close to the thickness of the S-layer and in this way might resemble the isoporous S-layer lattice. [4]

In summary, during the period covered by this annual report, a novel method for dispersing and coating pristine nanotubes with S-layer proteins was developed, on which all further work built. The binding properties of S-layer fusion proteins, which enable a highly specific functionalization of the MWNT surface, are essential and were used to bind gold-labeled antibodies to the corresponding binding domains of the S-layer fusion proteins. Materials science aspects have also been addressed through the binding of metallic nanoparticles and through the biomineralization of gold and silica. Although these are only a few examples of combining S-layer proteins and MWNTs in a construction kit, we would like to emphasize that our research, although longer term in nature, offers a new technology for functionalizing carbon nanotube surfaces and could eventually lead to new applications in biotechnology, medicine, and materials science.

The funding of the Austrian Science Fund (FWF), project P 31927-N28 is gratefully acknowledged.

References

[1] *A. Breitwieser, P. Siedlaczek, H. Lichtenegger, U.B. Sleytr, D. Pum,* S-Layer Protein Coated Carbon Nanotubes. *Coatings* 9 (2019) 492.

[2] *A. Breitwieser, U.B. Sleytr, D. Pum,* A New Method for Dispersing Pristine Carbon Nanotubes Using Regularly Arranged S-Layer Proteins. *Nanomaterials* 11/5 (2021) 1346.

[3] *D. Pum, A. Breitwieser, U.B. Sleytr,* Patterns in Nature - S-Layer Lattices of Bacterial and Archaeal Cells. Crystals 11/8 (2021) 869.

[4] *R. Tscheliessnig, A. Breitwieser, U.B. Sleytr, D. Pum,* Crystalline S-Layer Protein Monolayers Induce Water Turbulences on the Nanometer Scale. Crystals 11/9 (2021) 1147.

Hard plant shells: How cell walls determine tissue mechanics and functionality

Jessica C. Huss[1], Jakob Bachmayr[1], Sebastian J. Antreich[1], Nannan Xiao[1], Michaela Eder[2], Johannes Konnerth[3], Notburga Gierlinger[1]

[1]Institute of Biophysics, Department of Nanobiotechnology, University of Natural Resources and Life Science, Vienna, Austria
[2]Max Planck Institute of Colloids and Interfaces, Department of Biomaterials, Potsdam, Germany
[3]Institute of Wood Technology and Renewable Materials, Department of Material Sciences and Process Engineering, University of Natural Resources and Life Science, Vienna, Austria

Objective

The encapsulation of seeds in hard coats and fruit walls fulfils protective and dispersal functions in many plant families. In angiosperms, packaging structures possess a remarkable range of different morphologies and functionalities, as illustrated by thermo and hygro-responsive seed pods and appendages, as well as mechanically strong and water impermeable shells. Key to these different functionalities are characteristic structural arrangements and chemical modifications of the underlying tissues. Despite the abundance of hard plant shells, particularly nutshells, it remains unclear which fundamental properties drive their mechanical stability. Therefore, in this project, we explored how the tissue structure and composition affect the mechanical properties of hard plant shells.

Results & Conclusion

Sclerenchyma performs differently in static and responsive encapsulations due to the tissue arrangement, cell wall structure, and composition. If fibres are present, their orientation with respect to each other and their wall structure are important, because both parameters induce directionality (anisotropy) in terms of the mechanical properties and hygroscopic deformations. Broadly speaking, plants exploit fibre anisotropy for functional control, particularly for force generation. Consequently, we find fibrous tissues predominantly in responsive systems, whereas tissues in static encapsulations show a broader spectrum from entirely fibrous to nonfibrous. In static encapsulations, we found that the strongest tissues (in walnut and pistachio) exploit the topological interlocking of 3D-puzzle cells and thereby outperform the fiber-reinforced structure of macadamia under tensile and compressive loading. On the macroscopic scale, strengthening occurs via an increased shell thickness, spherical shape, small size, and a lack of extended sutures. These functional interrelations suggest that simple geometric modifications are a powerful and resource-efficient strategy for plants to enhance the fracture resistance of entire shells and their tissues.

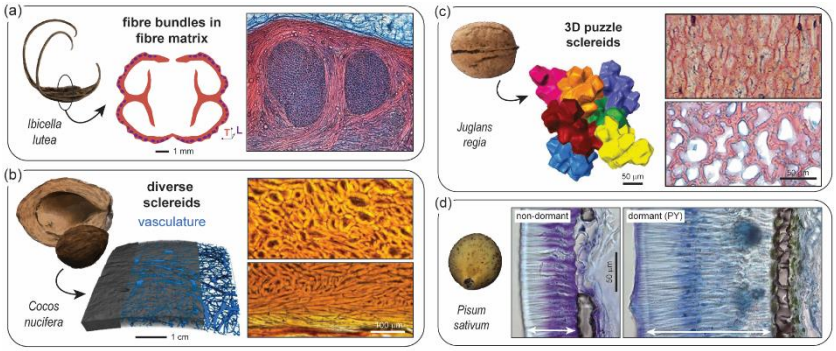

Figure 1: Anatomical features of hard, static seed encapsulations based on a-b) fibrous tissues; and c-d) non-fibrous tissues.

Huss JC, Gierlinger N (2021): Functional packaging of seeds. New Phytologist 230: 2154–2163. DOI: 10.1111/nph.17299

Twist and lock: nutshell structures for high strength and energy absorption

Nannan Xiao[1], Martin Felhofer [1], Sebastian J. Antreich[1], Jessica C. Huss[1], Konrad Mayer[1], Adya Singh[1], Peter Bock[1], Notburga Gierlinger[1]

[1]Institute of Biophysics, Department of Nanobiotechnology, University of Natural Resources and Life Science, Vienna, Austria

Objective

Walnut and pistaccio shells turned out to have both 3D-puzzle cells and remarkable mechanical properties. Pistaccio outperforms walnut shells by adding to high strength also high energy absortion. To unravel he reason for the superior performance of pistaccio shells we investigated both species on the cellular, micro-, nano-, and molecular levels using advanced imaging and tomography techniques.

Results & Conclusion

Due to numerous lobes (Figure 1), pistachio 3D puzzle cells contribute a 60-80% increased surface area per unit volume. These lobes interlock via ball-joint-like structures (Figure) and explain the excellent energy absorption and strain in tensile tests. In contrast, the brittle LEGO brick failure of the walnut shell goes hand in hand with numerous pit channels and three times higher lignin content. Atomic force with electron microscopy reveals a helicoidal architecture of cellulose macro fibrils within the cell wall. The pitch angle and thickness of these lamellae differ between the two species and explain the different mechanical properties even on the nanolevel.

In conclusion, cell shape, interlocking features, and the chemical composition of the different nut cell walls determine the mechanical protection capacity of the seed.

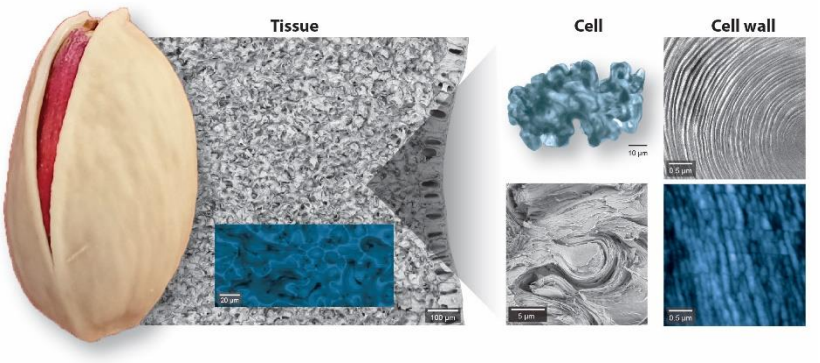

Figure 1: Scanning electron microscopy gives an overview of the tissue structure and confirms the same cell type across the entire shell. Raman imaging (blue inset) highlights lignin as glue between the cells and in the cell wall. Chemical isolation of single cell opens the view on the cell shape and highlights the numerous lobes and tremendous surface area. A zoom with electron microscopy reveals their interlocking by ball joint structures as well as the layered cell wall. Atomic force microscopy confirms the layering based on twisted cellulose fibrils.

Xiao N, Felhofer M, Antreich SJ, Huss JC, Mayer K, Singh A, Bock P, Gierlinger N (2019) Twist and lock: nutshell structures for high strength and energy absorption. Royal Society Open Science, 8: 210399. https://doi.org/10.1098/rsos.210399

Pistachios wallop walnuts as the toughest nut to crack | Science | AAAS

New materials based on waste: bacterial cellulose from kombucha production blended with walnut shells

Lilian Mira Kaufmann[1], Jessica Huss[1], Sebastian Antreich[1], Notburga Gierlinger[1]

[1]Institute of Biophysics, Department of Nanobiotechnology, University of Natural Resources and Life Science, Vienna, Austria

Abstract

The ever-growing demand for sustainable and bio-degradable materials bring into play several plant feedstock components. Especially cellulose as one of the most abundant polymers in nature, has shown high potential in the development of sustainable new materials due to its excellent mechanical properties.. Isolating cellulose from plant biomass often needs harsh chemical treatments as cellulose fibrils are intimately associated with hemicelluloses and lignin. In contrast bacterial cellulose can be easily produced via fermentation and meets today's needs for ecological green material manufacturing.

Utilizing waste to manufacture functional materials is the key scope of this research. Two waste components, bacterial cellulose from kombucha fermentation and walnut shells, are combined to produce sustainable composites. The bacterial cellulose pellicle grows at the air-liquid interface with easily controllable fermentation parameters (i.e. no aseptic working needed, fermentation media is easily cooked, etc.) and is finally a waste product of the kombucha industry. Walnut shells are also a waste product and currently often discarded or incinerated.

In this work, novel bacterial cellulose composite materials were produced with changing concentration of walnut shell cells as fillers. Characterisation of these sustainable composites included mechanical properties, water holding capacity and composite and surface structure and will help to assess the potential for various applications. Biomedical applications such as wound dressings might be interesting due to a high water holding capacity and long water retention times. Additionally, these composites might be used as a vegan leather-substitute or in the field of packaging materials.

Results & Conclusion

This work demonstrates how two waste components can be combined to generate a composite material with different amount of fillers (Figure 1) for manifold applications. The walnut shell cells showed good filler-behaviour within the bacterial cellulose fibril-network (Figure 1c-d). The addition of flexibility agents provides resilience for a broader area of application. The hardness and plasticity of the raw-materials could be combined in the composites (ranging from an average 4.43 to 1.51 MPa in the differently constituted composites). Nevertheless, tensile testings displayed high variability as can be seen in Figure 2.

Especially, the composite with 30 weight-% walnut shell cells (K-W30) is of interest for futures applications. It has good sewing capability, not only hand-sewing but also using a sewing-machine. The patches further stick together when utilizing normal glue (UHU extra). This provides for a wide variety of applications especially in the textile and fabric sector. Wallets as well as notebooks have been manufactured out of the material providing a unique appeal as well as wide applicability. Therefore, it can be used as a vegan leather substitute with an easier handling as it can be processed with more available tools such as normal sewing-machines and glue. Moreover, impregnation with

a berry wax-coconut oil mix adds hydrophobicity and broadens the applicability-spectrum even more.

The high water holding capacity (3.77 g/g for K-W30) might be useful in the biomedical-field, though proper sterilization is needed. But also in the package industry the hydrophilic character of the material patches can be utilized, since the packaging would attract water away from the item inside. Additionally, the re-moulding capacity could be of benefit for this sector, too. Packaging material provide a great source of waste, if these materials could be re-used in a broad way, a more circular economy would be possible.

Pictures/Figures

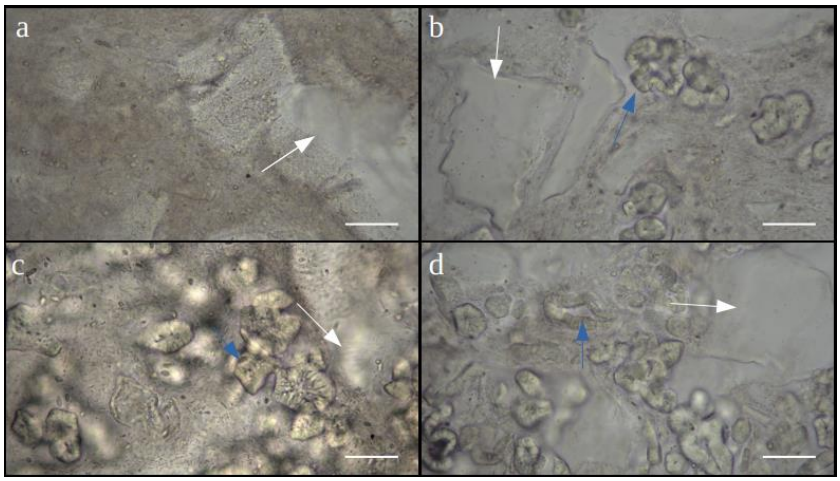

Figure 2: Light microscope picture (400x magnification, scale bars: 50 µm). White arrows point to agar-glycerol patches, blue arrows point to walnut shell cells (WSCs). a) without any added WSCs (K-0). b) 15 weight-% WSCs (K-W15). c) 30 weight-% WSCs (K-W30). d) 45 weight-% WSCs (K-W45).

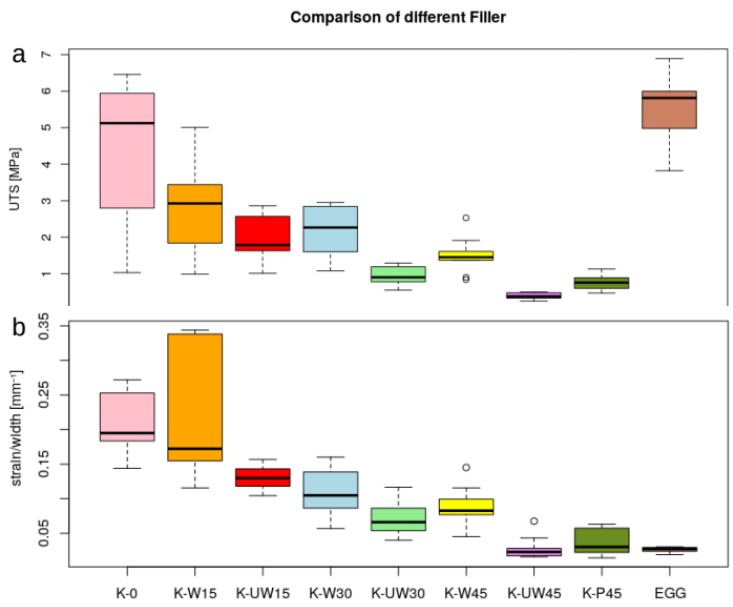

Figure 1: Tensile testing of composites with different filler. K-WX: main composites with X weight-% WSCs. K-UWX: composites with X weight-% walnut shell powder. K-P45: composite with 45 weight-% pine shell cells. EGG: egg carton box.

A belt for the cell: Cellulosic wall thickenings and their role in morphogenesis of the 3D puzzle cells in walnut shells

Sebastian J. Antreich[1], Nannan Xiao[1], Jessica C. Huss[1], Notburga Gierlinger[1]

[1]Institute of Biophysics, Department of Nanobiotechnology, University of Natural Resources and Life Science, Vienna, Austria

Objective

Mature walnut shells consist of polylobate sclereid cells, which interlock with all neighbour cells, so that the whole tissue resembles a 3D puzzle. The cells need to get shaped before secondary cell wall formation and lignification. To understand the cell morphogenesis of the polylobate sclereid cells we investigated the walnut shell tissue in the first three month of fruit development (Fig. 1A-E).

Results & Conclusion

Cell shaping occurs during the rapid growth phase, when the walnut increases its size, mainly through the expansion of the pericarp tissue. During this phase the cells change their shape from small isodiametric to large polylobate cells. For the shaping two features are important; turgor pressure and cell wall modifications. The turgor pressure pushes the cell walls against the neighbouring cells, like blowing up a balloon. However, the cell wall reinforces on places, which will become indents of the polylobate cell, with more cellulose fibrils (Fig. 1C). This cellulosic wall thickenings act like a belt against the turgor pressure, so that the cell wall expands there less strong than at other regions with minor cellulose deposition. This process stops with the onset of secondary cell wall formation and lignification. The findings show that simple modifications on the cell wall determine cell shape and finally result in the interlocked 3D-puzzle shell tissue.

Antreich SJ, Xiao N, Huss JC, Gierlinger N (2021) A belt for the cell: Cellulosic wall thickenings and their role in morphogenesis of the 3D puzzle cells in walnut shells. Journal of Experimental Botany 72(13):4744-4756. DOI: 10.1093/jxb/erab197)

Elbaum R, Elbaum M (2021) A tough 3D puzzle in the walnut shell Journal of Experimental Botany 72(13):4593-4595. DOI: 10.1093/jxb/erab221

Pictures/Figures

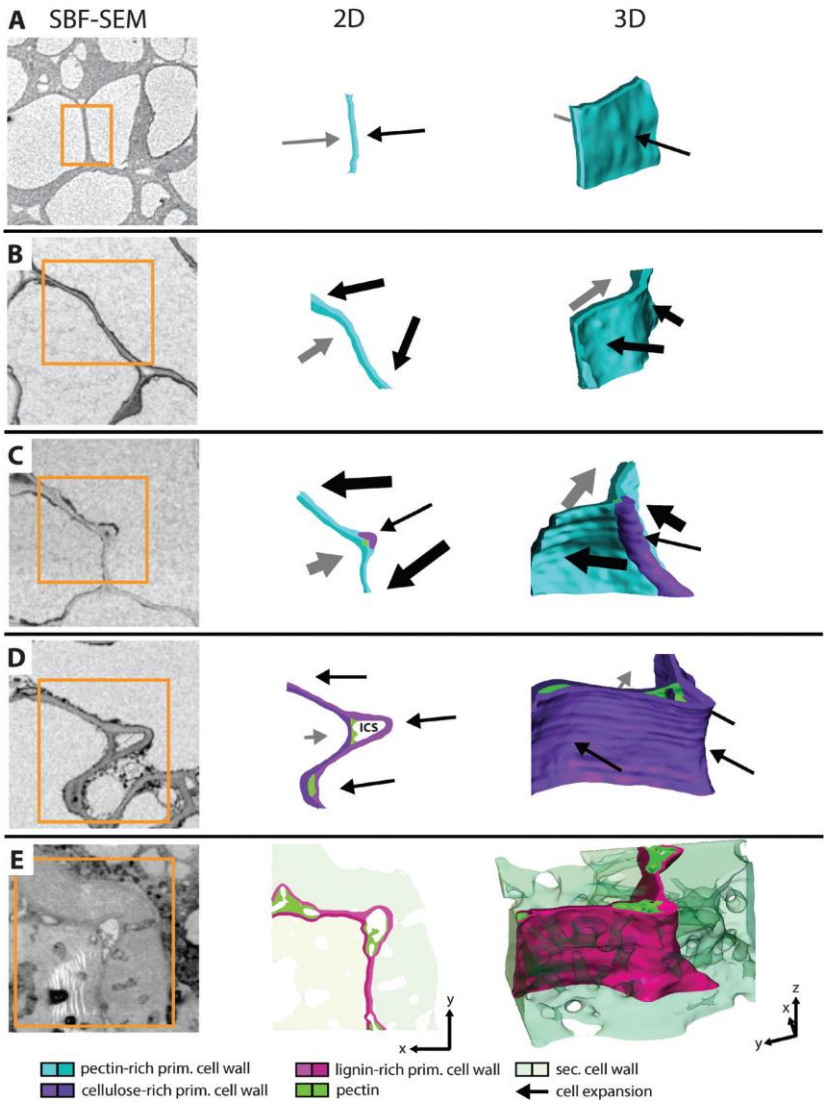

Fig. 1. Possible scenario for lobe formation of cells in walnut shell tissue. (A–E) Representative sections showed the cell wall of neighbouring cells in each developmental stage from SBF-SEM (same scaling), a 2D sketch, and a 3D visualization of the same area. (A) After cell division, the cell wall was straight and cell expansion should be still weak (thickness of arrows represents expansion speed and direction). (B) The cell expanded further, and the cell wall started to undulate, causing different expansion directions of the neighbouring cells. (C) Due to higher cell wall stresses at the curved section of the right cell, cellulose was deposited and the thickness increased at this location. The cell expanded further but less strongly at this position, and an indent started to form. A small intercellular space (ICS) is created, first filled completely. The opposite cell expanded off-plane and formed another loop of wall thickening. (D) Later during cell growth, the ICS became bigger and showed an open space, sometimes additionally protrusions. The whole cell wall became richer in cellulose and cells expanded less. (E) Finally, secondary cell wall was deposited, and the primary cell wall was lignified, which stopped the cell expansion.

Raman imaging of Micrasterias: new insights into shape formation

Martin Felhofer,[1] Konrad Mayer,[1] Ursula Lütz-Meindl,[2] Notburga Gierlinger

[1]Institute of Biophysics, Department of Nanobiotechnology, University of Natural Resources and Life Science, Vienna, Austria
[2]Department of Biosciences, University of Salzburg, 5020 Salzburg, Austria

Objective

The main objective of this work was to gain new insights into the cell shaping process of the unicellular green alga *Micrasterias*. Raman imaging, among other techniques, was applied to reveal chemical and structural changes in the cell wall, which is the basis for morphogenesis.

Results & Conclusion

The main finding is that cellulose (Figure) and pectin are the two most essential components of the cell wall to tune the stiffness and extensibility. Furthermore, the composition and alignment of micro-and nanofibrils are crucial to the non-uniform expansion and shaping of lobes.

In conclusion, the plant cell wall is not only a wall but also a dynamic feature with properties changing during development and locally along and across the cell wall.

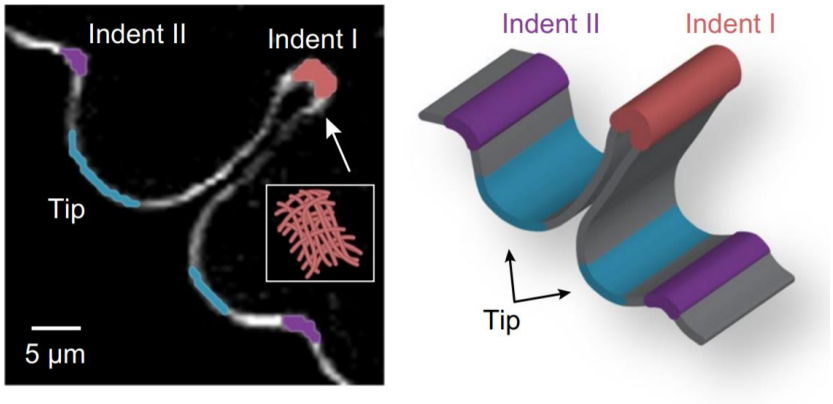

Figure | At the indents, cell wall thickening was observed, and cellulose has more contribution in the indents than in the tips. At the same time, hemicellulose (xyloglucan) was the main contributor at all three positions.

DOI: 10.1007/s00709-021-01685-3

A guide to elucidate the hidden multicomponent layered structure of plant cuticles by Raman imaging

Peter Bock[1], *Martin Felhofer*[1], *Konrad Mayer*[1] *and Notburga Gierlinger*[1]

[1]Institute of Biophysics, Department of Nanobiotechnology, University of Natural Resources and Life Science, Vienna, Austria

Objective

The cuticle covers almost all plant organs as the outermost layer and serves as a transpiration barrier, sunscreen, and first line of defense against pathogens. Waxes, fatty acids, and aromatic components build chemically and structurally diverse layers with different functionality. So far, electron microscopy has elucidated structure, while isolation, extraction, and analysis procedures have revealed chemistry. With this method paper, we close the missing link by demonstrating how Raman microscopy can give detailed information about chemistry and structure of the native cuticle on the microscale.

Results & Conclusion

We introduce an optimized experimental workflow, covering the whole process of sample preparation, Raman imaging experiment, data analysis, and interpretation and show the versatility of the approach on cuticles of a spruce needle, a tomato peel, and an Arabidopsis stem. We include laser polarization experiments to deduce the orientation of molecules and multivariate data analysis to separate cuticle layers and verify their molecular composition. Based on the three investigated cuticles, we discuss the chemical and structural diversity and validate our findings by comparing models based on our spectroscopic data with the current view of the cuticle. We amend the model by adding the distribution of cinnamic acids and flavonoids within the cuticle layers and their transition to the epidermal layer. Raman imaging proves as a non-destructive and fast approach to assess the chemical and structural variability in space and time. It might become a valuable tool to tackle knowledge gaps in plant cuticle research.

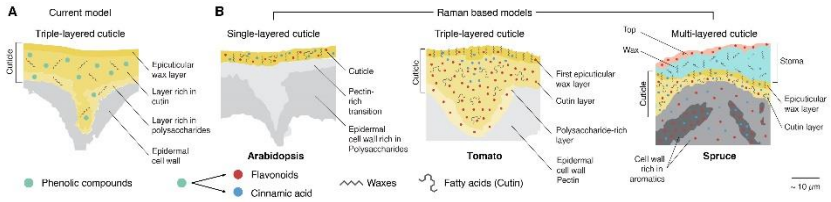

Fig.1. Expanding our view of the cuticle by Raman imaging. A) Current model of the cuticle mainly based on electron microscopy and wet chemistry. B) Models based on Raman imaging. Both layering and internal chemistry vary on the micro-scale and with species. Spectral analysis revealed common chemical compounds and design principles as well as species-specific variation.

Bock, P; Felhofer, Mayr K, Gierlinger, N (2021) A guide to elucidate the hidden multicomponent layered structure of plant cuticles by Raman imaging. Frontiers in Plant Science DOI: 10.3389/fpls.2021.793330

Sasani, N; Bock, P; Felhofer, M; Gierlinger, N (2021) Raman imaging reveals in-situ microchemistry of cuticle and epidermis of spruce needles. Plant Methods 17(1): 17. DOI: 10.1186/s13007-021-00717-6

Raman imaging reveals in-situ microchemistry of cuticle and epidermis of spruce needles

Nadia Sasani, Peter Bock, Martin Felhofer and Notburga Gierlinger

[1]Institute of Biophysics, Department of Nanobiotechnology, University of Natural Resources and Life Science, Vienna, Austria

Objective

In this study, we use Raman imaging and polarisation experiments to study the native cuticle and epidermal layer of needles of Norway spruce, one of the economically most important trees in Europe. The acquired hyperspectral dataset is the basis to image the chemical heterogeneity using univariate (band integration) as well as multivariate data analysis (cluster analysis and non-negative matrix factorization).

Results & Conclusion

Confocal Raman microscopy probes the cuticle together with the underlying epidermis in the native state and tracks aromatics, lipids, carbohydrates and minerals with a spatial resolution of 300 nm. A waxy, crystalline layer is discriminated on top (Fig. 1a-b), in which aliphatic chains and coumaric acid are aligned perpendicular to the surface. Also in the lipidic amorphous cuticle beneath, strong signals of coumaric acid and flavonoids are detected (Fig. 1c-d). At the interface between epidermis and cuticle Calcium oxalate crystals are detected (Fig. 1c-d). The underlying epidermal cell walls are devoid of lipids but show strong aromatic signals and weak carbohydrate bands (Fig. 1-h). Results sharpen our view about the cuticle as the outermost layer of plants and highlight the aromatic impregnation throughout.

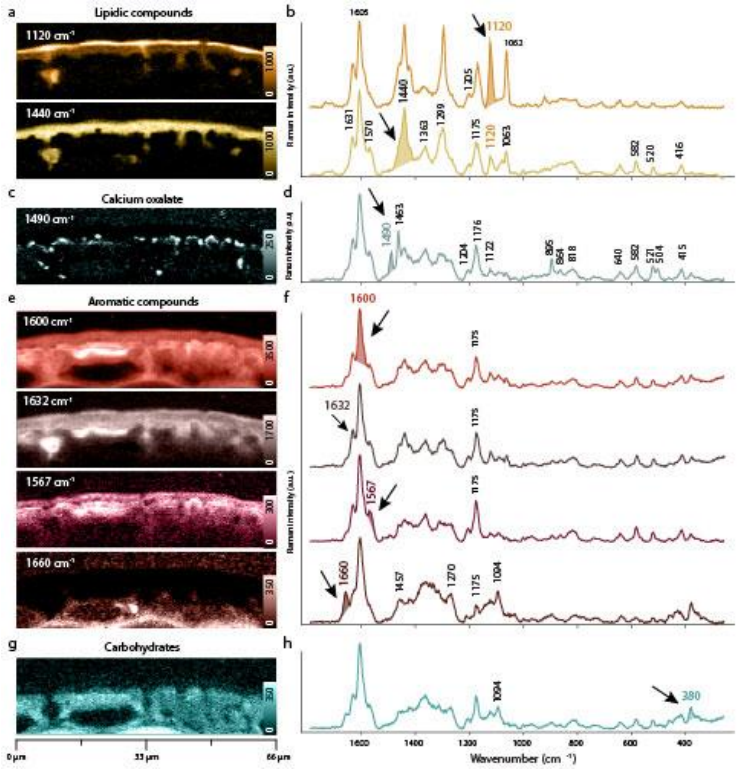

Figure 1.

Raman imaging of the cuticle of Norway spruce based on band integration and extracted average spectra
a) The outer lipidic layers are visualized by integrating the band at 1120 cm^{-1} and 1440 cm^{-1} and b) the extracted average spectra confirm the lipidic character
c) Integrating the band at 1490 cm−1 visualizes a pointwise accumulation of Calcium oxalate d) with bands at 1490, 1463 and 895 cm^{-1}.
e) Integrating different aromatic bands and f) extracted average spectra confirm aromatic dominance
g) Integrating the characteristic cellulose band at 380 cm^{-1} displays the epidermis andh) the derived average spectrum confirms carbohydrates together with aromatics.

Oak wood drying: precipitation of crystalline ellagic acid leads to discoloration

Martin Felhofer,[1] Peter Bock,[1] Nannan Xiao,[1] Christoph Preimesberger,[2] Martin Lindemann,[3] Christian Hansmann,[2] Notburga Gierlinger[1]

[1]Institute of Biophysics, Department of Nanobiotechnology, University of Natural Resources and Life Science, Vienna, Austria
[2]Institute of Wood Technology and Renewable Materials, Konrad Lorenz-Straße 24, 3430 Tulln, Austria; Wood K plus – Competence Centre for Wood Composites and Wood Chemistry, Konrad-Lorenz-Straße 24, 3430 Tulln
[3]Environmental and Bioscience Engineering, Institute of Chemical, Technische Universität Wien, Getreidemarkt 9, A-1060 Vienna, Austria

Objective

The strong color inhomogeneities of oakwood after drying are a long-standing and essential research question. We aimed to unravel the chemical changes on the micro-level of colored and uncolored areas to come up with a better understanding of the unwanted processes.

Results & Conclusion

The results showed precipitated crystalline ellagic acid in brighter areas, especially in rays, pits, and cell corners. These findings point to clogging of the water pathway and explain inhomogeneous moisture contents within the wood during drying. Moisture and temperature conditions change locally, and different hydrolysis and precipitation reactions of tannins occur.

Wood discolorations are a widespread problem in the lumber industry and cost millions of dollars each year. Therefore, wood technology and processing will benefit from this basic research study.

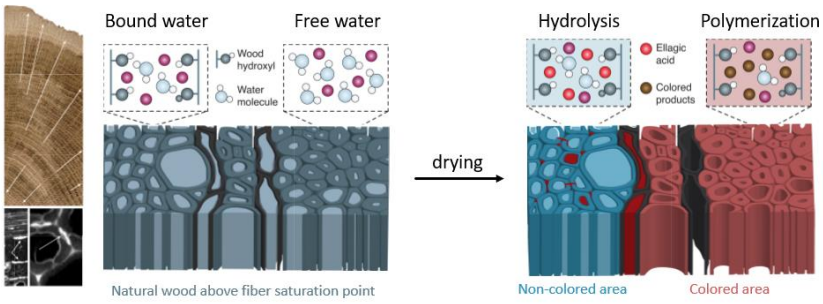

Figure 1. Oak wood microstructure with brighter areas (non-colored) and schematics of the changes during drying.

https://doi.org/10.1515/hf-2020-0170

Physiological and anatomical responses to drought stress differ between two larch species and their hybrid

Nadia Sasani[1], Luc E. Pâques[2], Guillaume Boulanger[3], Adya P. Singh[1], Notburga Gierlinger[1], Sabine Rosner[4] and Oliver Brendel[3]

[1]Institute of Biophysics, Department of Nanobiotechnology, University of Natural Resources and Life Science, Vienna, Austria
[2] INRAE, UMR BIOFORA, 45160 Ardon, France
[3] Université de Lorraine, Agro Paris Tech, INRAE, UMR Silva, 54000 Nancy, France
[4] Institute of Botany, University of Natural Resources and Life Sciences, Gregor Mendel Strasse 33, 1180 Vienna, Austria

Objective

The aim of our study was to compare the drought response of saplings of two larch species, European larch (EL) and Japanese larch (JL), and their hybrid (HL) under controlled drought conditions. The combination of these species was chosen, because European larch plays a major ecological role in, e.g., protection against snow and soil slides, and the hybrid of European and Japanese larch is of economical interest for timber production in plantations. We address two main research questions: first, did the hybrid inherit drought sensitivity from the Japanese larch, and second, which anatomical traits are responsible for lower drought sensitivity?

Results & Conclusion

Potential differences in drought sensitivity were examined with regard to whole plant transpiration response (plant water use, transpiration efficiency), biomass increase and wood formation. To infer hydraulic vulnerability, constitutive wood anatomy (anatomy before drought stress) including pit structural parameters was analyzed. Differences in wood anatomy were analysed in 5% steps along the latest radial increment. Stressed trees showed a decrease in radial lumen starting at about 50% of the increment for all species. When lumen diameters were plotted against the absolute distance from pith to bark (tracheidograms); the extreme reaction of HL to drought stress became obvious. In addition to a decrease in radial increment, lumen diameters decreased (Figure 1). In the region of the last 90–95% of the increment, radial lumen diameters significantly decreased due to drought in all species, but drought stressed EL had significantly larger lumens than stressed HL and JL. Young saplings of the three larch species (EL, JL and HL) adopted different strategies towards drought. For the European larch, we hypothesize that its slower growth is associated with a hydraulically safer wood design, allowing a more anisohydric strategy, whereas a less safe design in the Japanese larch and the hybrid demands stronger stomatal control and thus a more isohydric strategy. We conclude that the HL was inherited their strategy towards drought stress from JL rather than from EL. The anisohydric (drought response) strategy of EL could allow a range shift under climate change from its native range to higher elevations or regions that are more northern. The observed higher growth of HL, even under drought, and its higher resistance against diseases, supports its inclusion in pure and mixed lowland plantations in regions, where EL is native.

https://doi.org/10.1007/s00468-021-02129-4

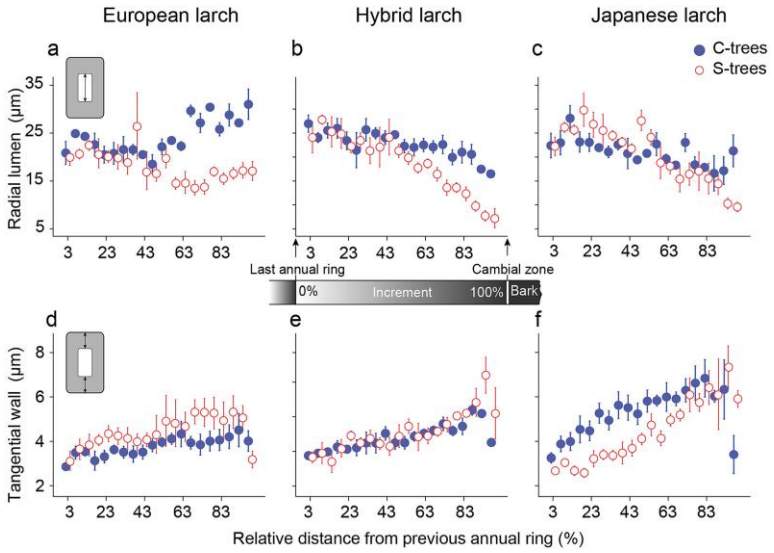

Figure 2. Tangential wall thickness and radial lumen diameter in 5% steps of the 2015 increment of European, hybrid and Japanese larch trees with two treatments (control and drought stress). Each stepwise mean value of radial lumen diameter of European larch (a), hybrid larch (b), and Japanese larch (c), and tangential wall thickness of European larch (d), hybrid larch (e), and Japanese larch (f) is shown with standard deviation for the two treatments “control” (C-trees, closed symbols) and drought stressed trees (S-trees, open symbols). Whiskers indicate the standard deviation.

Raman spectroscopy reveals collagen and phospholipids as major components of hyalinosis in the arteriolosclerotic ulcer of Martorell

J. Deinsberger,[1,2] M. Felhofer,[3] J.P. Kläger,[4] P. Petzelbauer,[1,2] N. Gierlinger,[3] B. Weber[1,2]

[1]Skin and Endothelium Research Division (SERD), Department of Dermatology, Medical University of Vienna, Vienna, Austria
[2]Department of Dermatology, Vienna General Hospital, Medical University of Vienna, Vienna, Austria
[3]Institute of Biophysics, Department of Nanobiotechnology, University of Natural Resources and Life Sciences Vienna (BOKU), Vienna, Austria
[4]Department of Pathology, Vienna General Hospital, Medical University of Vienna, Vienna, Austria

Objective

The aim of this study was the molecular characterization of hyaline arteriolar deposits in patients with hypertensive arteriolopathy by confocal Raman spectroscopy.

Results & Conclusion

Raman microspectroscopy revealed subendothelial hyaline deposits in arteriolosclerotic ulcers composed of collagen and phospholipids, particularly phosphatidylcholine. Additionally, in hypertensive nephrosclerosis, collagen is also present. Furthermore, actin decreases in the process of hyalinization, corresponding to the loss of smooth muscle cells.

The results suggest that hyaline deposition in arterioles in hypertensive arteriolopathy and the absence of actin intimate that potentially critical disease mechanisms involve pressure-induced apoptosis of vascular smooth muscle cells with subsequent collagen deposition (Figure).

Pictures/Figures

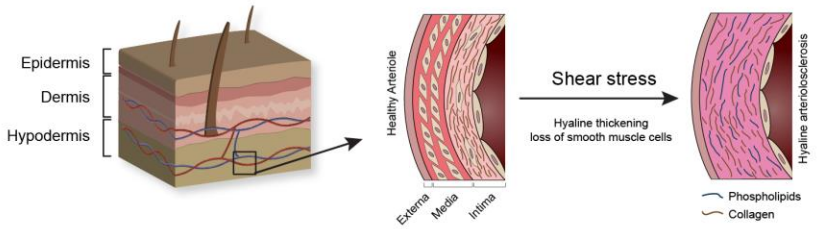

Figure | Schematic representation of a healthy arteriole and an arteriosclerotic arteriole, with changes induced by the continuously elevated shear stress of the deep cutaneous plexus, is at the dermal/hypodermal junction.

2021 - Journal of the European Academy of Dermatology and Venereology - Wiley Online Library: https://doi.org/10.1111/jdv.17573

Cell stiffness under small and large deformations: effects of actin disruptors CK-869 and jasplakinolide

S. Zemljic-Jokhadar[1], Jagoba Iturri, José L. Toca-Herrera, J. Derganc[1]

[1]Institute of Biophysics, Faculty of Medicine, University of Ljubljana, Vrazov trg 2, SI-1000 Ljubljana, Slovenia

Cytoskeleton-disrupting drugs can have different effects on cell mechanics at different deformation scales. We therefore applied two complementary indentation techniques to study the effects of two actin-disrupting drugs on cellular stiffness of human umbilical vein endothelial cells. Optical tweezers were used to probe the cortical stiffness at small deformations, and atomic force microscopy was used to probe the bulk cell stiffness at larger deformations. The first drug studied was CK-869, which is an inhibitor of the actin branching complex Arp2/3, and has not been analysed yet in terms of mechanical effects. A significant decrease in cell stiffness upon treatment with CK-869 was measured with both techniques, which implies that actin branching is important for cell mechanics at small and large deformations. The second drug studied was jasplakinolide, for which ambiguous effects on cell mechanics have been reported. In line with previous studies, we found that jasplakinolide caused significant cell stiffening at large deformations but slight cell softening under small deformations. This result implies that jasplakinolide has different effects on different levels of actin organization.

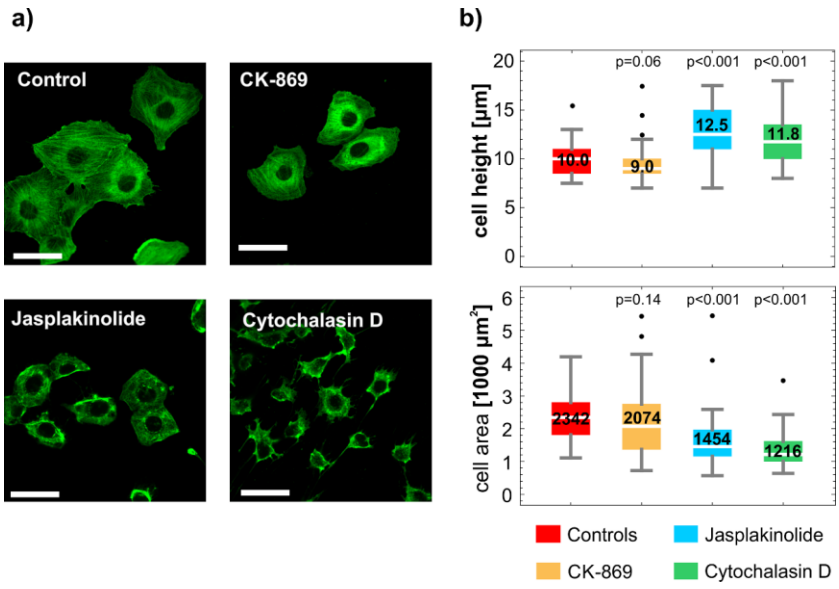

Figure 1: Effects of the treatments of HUVEC cells on actin distribution (a) and cell size (b). (a) Basal confocal sections of control and treated cells labelled with anti-β-actin. The scale bar represents 50 µm. (b) Cell height and adhered cell area. Boxes span over 50% of the measurements, the white horizontal lines represent the medians, and the dots represent the outliers. For each treatment, the median value is indicated in the box, and the p-value describing the difference relative to the control is presented at the top. The number of measured cells was 42 in all cases. The measurements were performed with confocal microscopy on cells labelled by wheat germ agglutinin (WGA) Alexa Fluor 488 conjugate.

Nucleotides-Induced Changes in the Mechanical Properties of Living Endothelial Cells and Astrocytes

Juan Carlos Gil-Redondo, Jagoba Iturri, F. Ortega [1], R. Pérez-Sen [1], Andreas Weber, M.-T. Miras-Portugal [1], José Luis Toca-Herrera, E. G. Delicado [1]

[1]Departamento de Bioquímica y Biología Molecular, Facultad de Veterinaria, Instituto Universitario de Investigación en Neuroquímica (IUIN), Instituto de Investigación Sanitaria del Hospital Clínico San Carlos (IdiSSC), Universidad Complutense Madrid, 28040 Madrid, Spain

Endothelial cells and astrocytes preferentially express metabotropic P2Y nucleotide receptors, which are involved in the maintenance of vascular and neural function. Among these, P2Y1 and P2Y2 receptors appear as main actors, since their stimulation induces intracellular calcium mobilization and activates signaling cascades linked to cytoskeletal reorganization. In the present work, we have analyzed, by means of atomic force microscopy (AFM) in force spectroscopy mode, the mechanical response of human umbilical vein endothelial cells (HUVEC) and astrocytes upon 2MeSADP and UTP stimulation. This approach allows for simultaneous measurement of variations in factors such as Young's modulus, maximum adhesion force and rupture event formation, which reflect the potential changes in both the stiffness and adhesiveness of the plasma membrane. The largest effect was observed in both endothelial cells and astrocytes after P2Y2 receptor stimulation with UTP. Such exposure to UTP doubled the Young's modulus and reduced both the adhesion force and the number of rupture events. In astrocytes, 2MeSADP stimulation also had a remarkable effect on AFM parameters. Additional studies performed with the selective P2Y1 and P2Y13 receptor antagonists revealed that the 2MeSADP-induced mechanical changes were mediated by the P2Y13 receptor, although they were negatively modulated by P2Y1 receptor stimulation. Hence, our results demonstrate that AFM can be a very useful tool to evaluate functional native nucleotide receptors in living cells.

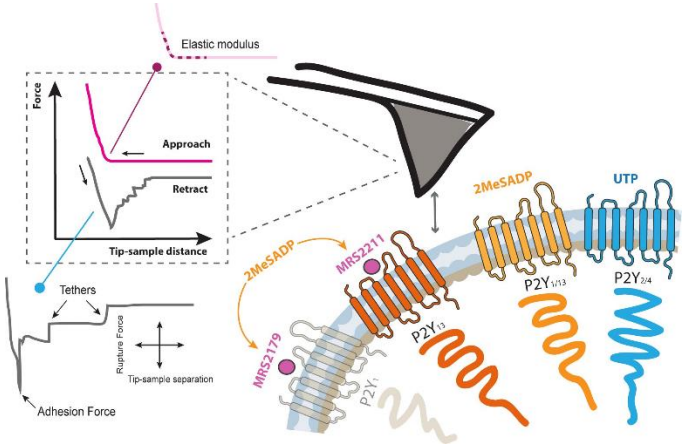

Figure: Graphical scheme of the performed experiments: (left) Mechanics-related factors extracted from the raw Force vs distance plots. (Right) Diagram showing the membrane of cerebellar astrocytes and the different purinergic receptors under analysis.

Mechanical response of cerebellar astrocytes upon selective stimulation/blocking of the purinergic receptor P2X7

Jagoba Iturri, Juan Carlos Gil-Redondo, M.-T. Miras-Portugal[1], E. G. Delicado [1], José L. Toca-Herrera, F. Ortega [1]

[1] Departamento de Bioquímica y Biología Molecular, Facultad de Veterinaria, Instituto Universitario de Investigación en Neuroquímica (IUIN), Instituto de Investigación Sanitaria del Hospital Clínico San Carlos (IdiSSC), Universidad Complutense Madrid, 28040 Madrid, Spain

Objective

Nucleotides act as extracellular messengers regulating a vast amount of functions, and their effects are mediated by membrane receptors known as P2 receptors. P2 receptors are classified into two different groups: P2Y and P2X receptors. P2Y receptors are G-protein coupled receptors activated by adenine and uracil tri- and diphosphates, while P2X receptors are ATP-gated cationic channels. In this work our efforts are focused on unravelling the role of these P2X7 nucleotide receptors from Rat cerebellar astrocytes. It is already known that the signaling of these ionotropic receptors also include metabotropic pathways independent from the ionic channel activity, such as MAP kinases ERK1/2 and protein kinase D (PKD). Interestingly, while activation of ERK1/2 kinases by $P2Y_2$/$P2Y_4$ receptors induce migration of the astrocytes, activation of these kinases by P2X7 receptors cause complex changes in cell morphology. Therefore, changes in the cytoskeleton and mechanical properties of the cell are to be expected.

Results & Conclusion

Stimulation of P2X7 receptors of rat cerebellar astrocytes with the selective agonist BzATP increases the stiffness of the cells. Treatment with the competitive antagonist of P2X7R, A-438079, does not block the increase in stiffness caused by the agonist, pointing that the effects observed are not dependent on the ionotropic activity of the receptor, but rather effects of the independent metabotropic pathways that are not blocked by the antagonist. Similar results are obtained when analyzing the viscous moduli of astrocytes, indicating possible changes in the cytoskeleton that are not blocked by the antagonist. Force spectroscopy maps of the cells show higher stiffness values and stronger adhesive forces throughout all the cytoplasm after treatment with the agonist, further supporting the evidence of changes in the cytoskeleton.

Treatment	E_{app} (kPa) ± SE	η_1 (Pa s) ± SE	η_2 (Pa s) ± SE
Control	4.84 ± 0.43	31.9 ± 2.3	590.8 ± 52.6
BzATP	5.93 ± 0.42	44.9 ± 3.2	1171.2 ± 118.1
A43	4.03 ± 0.26	31.8 ± 1.9	680.1 ± 60.1
A43 + BzATP	8.60 ± 0.91	50.4 ± 5.9	1774.9 ± 285.7

Table. Effects of P2X7 agonist/antagonist treatment on the apparent Young's modulus (Eapp) and viscosity of Maxwell elements 1 and 2 (η1 and η2) of rat cerebellar astrocytes. Notice that, for all the parameters, treatment with the antagonist A43 seems to further increase the effects caused by the treatment with the agonist BzATP (highlighted in blue).

Time- and Zinc-Related Changes in Biomechanical Properties of Human Colorectal Cancer Cells Examined by Atomic Force Microscopy

M. Maares[1], C. Keil [1], L. Löher [1], Andreas Weber, Amsatou Andorfer-Sarr, H. Haase [1], Jagoba Iturri, José Luis Toca-Herrera

[1]Chair of Food Chemistry and Toxicology, Technische Universität Berlin, Straße des 17. Juni 135, 10623 Berlin, Germany

Monitoring biomechanics of cells or tissue biopsies employing atomic force microscopy (AFM) offers great potential to identify diagnostic biomarkers for diseases, such as colorectal cancer (CRC). Data on the mechanical properties of CRC cells, however, are still scarce. There is strong evidence that the individual zinc status is related to CRC risk. Thus, this study investigates the impact of differing zinc supply on the mechanical response of the in vitro CRC cell lines HT-29 and HT-29-MTX during their early proliferation (24–96 h) by measuring elastic modulus, relaxation behavior, and adhesion factors using AFM. The differing zinc supply severely altered the proliferation of these cells and markedly affected their mechanical properties. Accordingly, zinc deficiency led to softer cells, quantitatively described by 20–30% lower Young's modulus, which was also reflected by relevant changes in adhesion and rupture event distribution compared to those measured for the respective zinc-adequate cultured cells. These results demonstrate that the nutritional zinc supply severely affects the nanomechanical response of CRC cell lines and highlights the relevance of monitoring the zinc content of cancerous cells or biopsies when studying their biomechanics with AFM in the future.

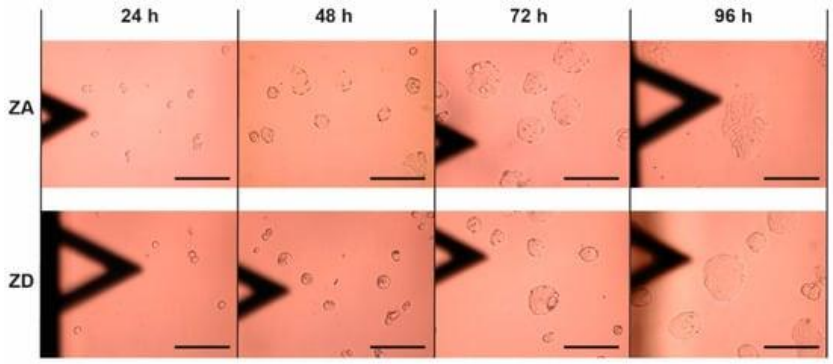

Figure: Graphical scheme of the performed experiments: (left) Mechanics-related factors extracted from the raw Force vs distance plots. (Right) Diagram showing the membrane of cerebellar astrocytes and the different purinergic receptors under analysis.

Mechanical Properties of alginate-based aerogels upon buffer-dependent swelling

Jagoba Iturri [1], C, Keil [2], H, Haase [2], José Luis Toca-Herrera [1]

[1] Institute of Biophysics, Department of Nanobiotechnology, University of Natural Resources and Life Science, Vienna, Austria
[2] Chair of Food Chemistry and Toxicology, Technische Universität Berlin, Straße des 17. Juni 135, 10623 Berlin, Germany

The mechanical response of Ca-Zn-Ag containing Alginate Aerogels was tested upon swelling in different buffers (water, HEPES, SBF, SBF-Albumin). Mechanical properties were measured by application of force mappings over large scan areas (25-100 μm²) at constant loading force and rates. The overall collection of individual mechanical factors (e.g. adhesion, sample stiffness -the value of the slope-) for each of the cases under study, was then analyzed statistically for comparative purposes. Figure below shows the resulting trend from comparing dry (purple) and wet (in water, red) specimens, with an enormous drop in the elastic modulus of the gels (in the shape of thin films on glass) as they were exposed to the swelling liquid.

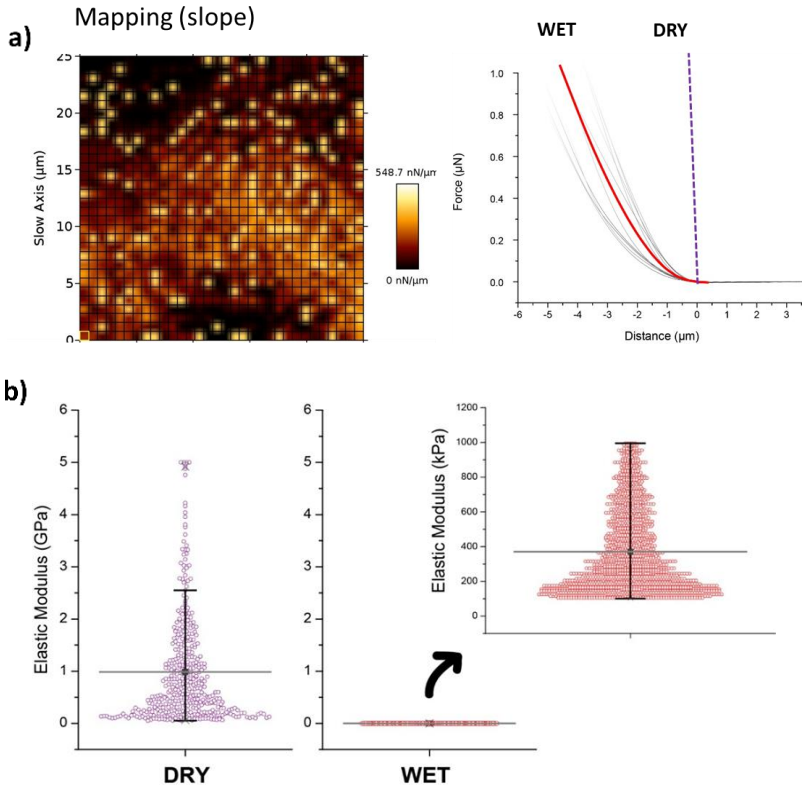

Figure: (a) Representative mapping of stiffness (slope) values for a random scanned area. The force distance plots on the right show the calculation of the average approach plot (in red) of the indented aerogel in wet conditions. The almost perpendicular dashed line acts as reference for the plot obtained in dry conditions. (b) Statistical analysis of the individual values (N > 800) obtained for the elastic modulus of the aerogel in both dry (purple) and wet (red) conditions. The inset magnifies the scale for the wet case. Grey line indicates the median, while the whiskers refer to the 5-95 level.

Characterization of the mechanical behavior and macrophage-mediated degradation of degradable, electrospun poly-urethane vascular grafts

M. Enayati [1,2], S. Puchhammer [1], Jagoba Iturri, C. Grasl [2,3], C. Kaun [4], S. Baudis [5], I. Walter [6], H. Schima [2,3], R. Liska [5], J. Wojta [2,4], Jose Luis Toca-Herrera, B. K. Podesser [1,2], H. Bergmeister [1,2]

[1] Center for Biomedical Research, Medical University of Vienna, Vienna, Austria
[2] Ludwig Boltzmann Institute for Cardiovascular Research, Vienna, Austria
[3] Center for Medical Physics and Biomedical Engineering, Medical University of Vienna, Austria
[4] Division of Internal Medicine II, Medical University Vienna, Austria
[5] Institute of Applied Synthetic Chemistry, Technische Universitat ¨ Wien, Vienna, Austria
[6] Department of Pathobiology, Veterinary University, Vienna, Austria

In this study, the degradation, macro-/micro-mechanical behavior and inflammatory behavior of a novel biodegradable scaffold composed of thermoplastic polyurethane (TPU) was characterized upon *in vitro* exposure to macrophages over an extended period of time. TPU scaffolds were fabricated via electrospinning, which yielded fibrous scaffolds with an average fiber diameter of 1.39 ± 0.76 µm and an average pore size of 7.5 ± 1.1 µm. Results showed that TPU scaffolds supported the attachment and migration of macrophages throughout the three-dimensional matrix. Scaffold degradation could be detected in localized areas, emphasizing the role of adherent macrophages in scaffold degradation. Weight loss, molecular weight and biomechanical strength reduction were evident in the presence of primary macrophage cells.

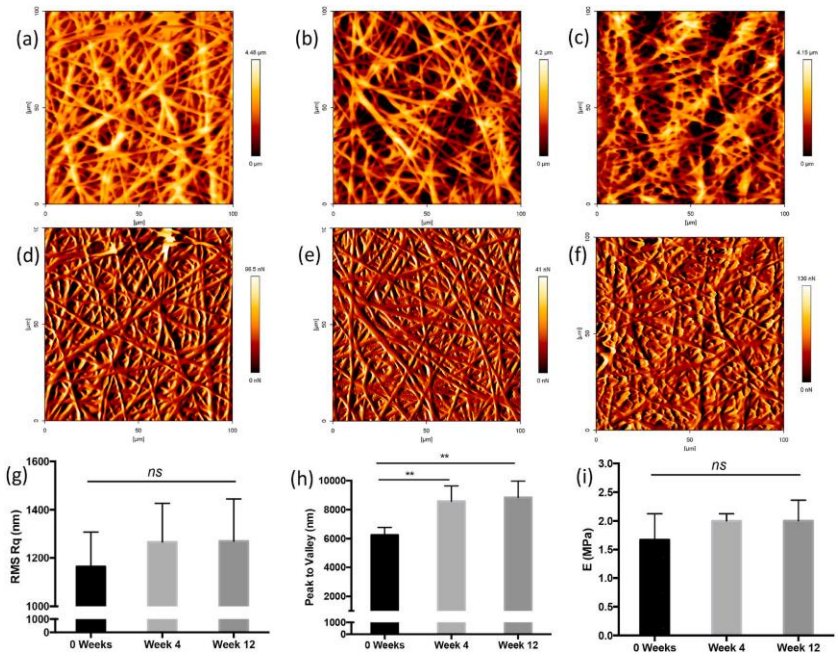

Figure: Representative AFM microscopy (a–c) height and (d–f) vertical deflection images (100 × 100 µm) of the macrophage seeded TPU grafts at different time points (0, 4, 12 weeks), (g & h) surface Roughness (RMS Rq) and peak to valley measurements, (i) Calculated Young's modulus (E) values via indentation measurements. Data represent mean ± S.D. n = 5 per time point (technical replicates: 3), **: $p < 0.001$, ns: not significant.

Nanostructured scaffolds based on bioresorbable polymers and graphene inducing aligned migration and accelerated neuronal differentiation of neural stem cells

Y. Polo[1], J. Luzuriaga, [2], Jagoba Iturri, I. Irastorza, [2], José Luis Toca-Herrera, G. Ibarretxe [2], F. Unda [2], J.-R. Sarasua [3], J.-R. Pineda [2,4], A. Larrañaga [3]

[1] Polimerbio SL, Donostia-San Sebastian, Spain
[2] Department of Cell Biology and Histology, Faculty of Medicine and Nursing, University of the Basque Country (UPV/EHU), Leioa, Spain
[3] Group of Science and Engineering of Polymeric Biomaterials (ZIBIO Group), Department of Mining, Metallurgy Engineering and Materials Science & POLYMAT, University of the Basque Country (UPV/EHU), Bilbao, Spain
[4] Achucarro Basque Center for Neuroscience, University of the Basque Country (UPV/EHU), Leioa, Spain

In this study, we fabricated bioresorbable elastomeric scaffolds combining an ordered nanopatterned topography together with a surface functionalization with graphene oxide (GO) in mild conditions. These scaffolds allowed the attachment of murine neural stem cells (NSCs) without the need of any further coating of its surface with extracellular matrix adhesion proteins. The NSCs were able to give rise to both immature neurons and supporting glial cells over the nanostructured scaffolds in vitro, promoting their aligned migration in cell clusters following the nanostructured grooves. This system has the potential to reestablish spatially oriented neural precursor cell connectivity, constituting a promising tool for future cellular therapy including nerve tissue regeneration.

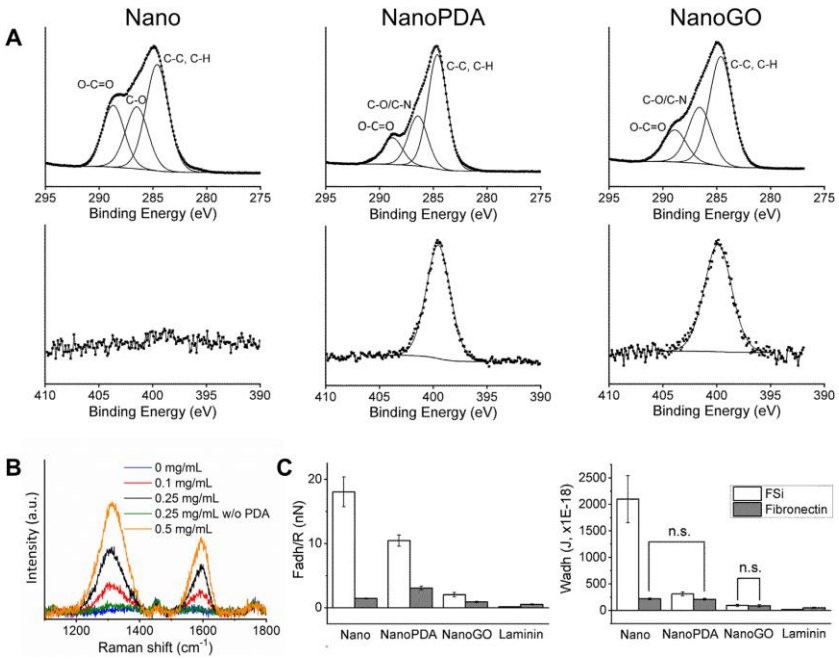

Figure: Surface characterization of the scaffolds. (A) High resolution C 1 s (top) and N 1 s (bottom) XPS spectra of nanostructured PLCL (Nano), nanostructured PLCL coated with PDA (NanoPDA) and further functionalized with GO (NanoGO). (B) Raman spectra of NanoGO scaffolds at different concentrations of GO solution. (C) Mean adhesion force (left) and work of adhesion (right) values for FSi (white) and fibronectin-coated (gray) probes. The error bars correspond to the standard error of the mean (SEM). Statistically significant differences ($P < 0.05$) were observed in all the cases, except in those indicated by n.s.

Single-Cell Probe Force Studies to Identify Sox2 Overexpression-Promoted Cell Adhesion in MCF7 Breast Cancer Cells

Jagoba Iturri, Andreas Weber, Maria dM Vivanco [1], José Luis Toca-Herrera

[1] Cancer Heterogeneity Lab, Center for Cooperative Research in Biosciences (CIC bioGUNE), Basque Research and Technology Alliance (BRTA), Bizkaia Technology Park, 48160 Derio, Spain

The replacement of the cantilever tip by a living cell in Atomic Force Microscopy (AFM) experiments permits the direct quantification of cell–substrate and cell–cell adhesion forces. This single-cell probe force measurement technique, when complemented by microscopy, allows controlled manipulation of the cell with defined location at the area of interest. In this work, a setup based on two glass half-slides, a non-fouling one with bacterial S-layer protein SbpA from L. sphaericus CMM 2177 and the second with a fibronectin layer, has been employed to measure the adhesion of MCF7 breast cancer cells to fibronectin films (using SbpA as control) and to other cells (symmetric vs. asymmetric systems). The measurements aimed to characterize and compare the adhesion capacities of parental cells and cells overexpressing the embryonic transcription factor Sox2, which have a higher capacity for invasion and are more resistant to endocrine therapy in vivo. Together with the use of fluorescence techniques (epifluorescence, Total Internal Fluorescence Microscopy (TIRF)), the visualization of vinculin and actin distribution in cells in contact with fibronectin surfaces is enabled, facilitating the monitoring and quantification of the formation of adhesion complexes. These findings demonstrate the strength of this combined approach to assess and compare the adhesion properties of cell lines and to illustrate the heterogeneity of adhesive strength found in breast cancer cells.

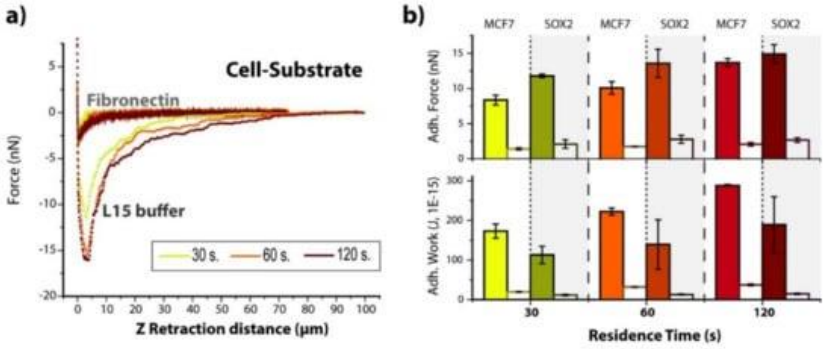

Figure: Influence of soluble fibronectin. (a) Representative force–distance plots for Sox2 cells interacting with Fibronectin substrates in L15 medium either with or without fibronectin addition, and increasing contact times (30, 60 and 120 s). (b) Calculated values of maximum adhesion force and adhesion work for both MCF7 and Sox2 cells before (filled columns, values from Figure 2) and after (empty columns) the injection of soluble fibronectin.

Characterizing the early-stage cell-cell and cell-substrate adhesion of MCF7 and HEK-293 cells

Dominik Wiesinger, Jagoba Iturri, Amsatou Andorfer-Sarr, José Luis Toca-Herrera

The use of a living cell as measuring probe in the so-called Single-Cell Probe Force Spectroscopy methodology, enables the measurement and quantification of earliest cell-cell and cell-substrate interactions. Furthermore, the broad choice in cell types, substrates, and measuring conditions (presence/absence of drugs or other (bio)molecules) provides multiple possibilities for experiment design.

In this work, for instance, the adhesive behavior of MCF-7 (breast cancer) and HEK-293 cells (Embrionary Kidney cells, usual model cell line for kidney tumor cells) onto clean glass substrates and to underlying (homotypic) cells was compared, known the large invasiveness differences shown by both cell lines. The resulting adhesion was measured for eight different residence times (0, 5, 10, 20, 30, 60, 90 and 120 s), thus covering the range from first attachment up to the pre-establishment of tighter connections, while loading force and pulling rate (approach and retract) are kept constant. First results showed an exponentially growing dependence of adhesion factors with the residence time under both cell-substrate and cell-cell interactions, with remarkable differences in the maximum values obtained depending on the cell line under analysis.

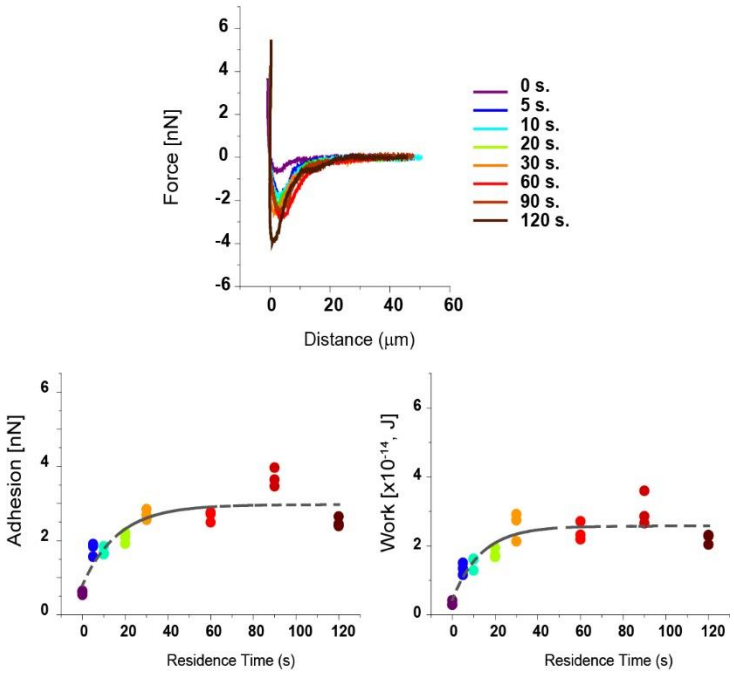

Figure: (Top) Residence time-dependent Force vs distance plots for the retraction segment of HEK293 cell-cell contact, and (Bottom) corresponding Maximum adhesion force - in nN, left- and Adhesion Work - in $x10^{-14}$ J, right- values extracted from similar plots. The dashed grey line shows the data fitting performed with an exponential equation of first order.

Fabrication of hierarchical Polymer-based niches for enhanced cell attachment

Jagoba Iturri, Hannah Blaschka, Amsatou Andorfer-Sarr, José Luis Toca-Herrera

Controlling and understanding adhesion of cells on artificial surfaces remains as a critical topic in materials and life sciences. In this regard, combination of top-down (contact printing) and bottom-up approaches (ATRP polymerization + layer-by-layer adsorption of polyelectrolytes and proteins) appears as a promising strategy for the design and fabrication of cell-appealing interfaces. Interestingly, this methodology allows going from 2D to 3D-like hierarchical structures of hybrid content (niches) that influence a subsequent cell attachment on top, by better exposing the specific binding sites (RGD, IKVAV moieties) towards target membrane receptors (i.e. integrins, CD44). Complementary use of Atomic Force Microscopy (AFM), with a living cell as probe, together with Quartz Crystal Microbalance with Dissipation (QCM-D) techniques, enable an early-stage analysis and quantification of these cell-substrate interactions on the nanoscale.

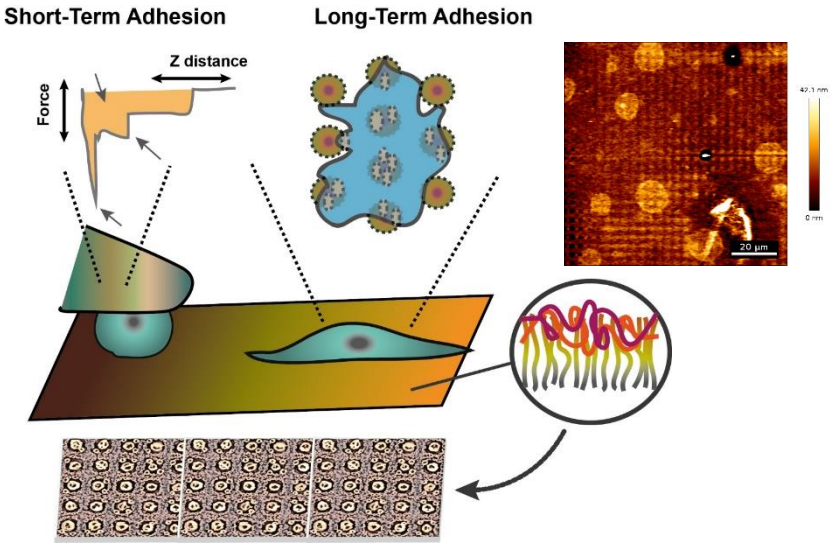

Figure: Graphical scheme showing the experimental arrangement for the different adhesion range (short-term vs long-term). The input shows an AFM imaging example of one of the systems built, in which the yellow circles correspond to fibronectin discs on top of pre-built polymer brushes.

Effects of substrate elasticity on the viscoelastic properties of MCF-7 cells

Juan Carlos Gil-Redondo[1], Andreas Weber[1], Barbara Zbiral[1], Maria dM. Vivanco[2], José L. Toca-Herrera[1]

[1]Institute of Biophysics, Department of Nanobiotechnology, University of Natural Resources and Life Science, Vienna, Austria
[2]Cancer Heterogeneity Lab, CIC bioGUNE, Bizkaia Science and Technology Park, 48160 Derio, Spain

Objective

Cells sense stiffness of surrounding tissues and adapt their activity, proliferation, motility and mechanical properties based on such interactions. Cancer and other diseases alter stiffness of tissues, and the response of cancer cells to this stiffness can also be affected. The goal of this study was to analyse the effects of substrate elasticity on the mechanical properties of MCF-7 breast cancer cells. For this, MCF-7 cells were plated on polyacrilamide gels of varying stiffness (0.1 – 264 kPa) and their elastic and viscoelastic properties were measured using Atomic Force Microscopy (AFM). The Apparent Young's Modulus was derived from the indentation of the cells, while a second exponential decay was used to fit the stress-relaxation pause segment in order to calculate the viscoelastic parameters based on a Zener model of the cell. Confocal microscopy was employed to visualize the morphology and actin cytoskeleton of the cells.

Results & Conclusion

MCF-7 cells seeded on polyacrylamide gels have the ability to detect the stiffness of the substrate and alter their mechanical properties in response. MCF-7 cells plated on soft substrates display lower stiffness and viscosity when compared to those seeded on stiffer gels or glass. These differences can be associated with differences in the morphology and cytoskeleton organisation, since cells seeded on soft substrates have a round morphology while cells seeded on stiffer substrates acquire a flat and spread morphology with formation of actin filaments, similar to that observed when seeded on glass. These findings show that MCF-7 cells can detect the stiffness of the surrounding microenvironment and thus, modify their mechanical properties.

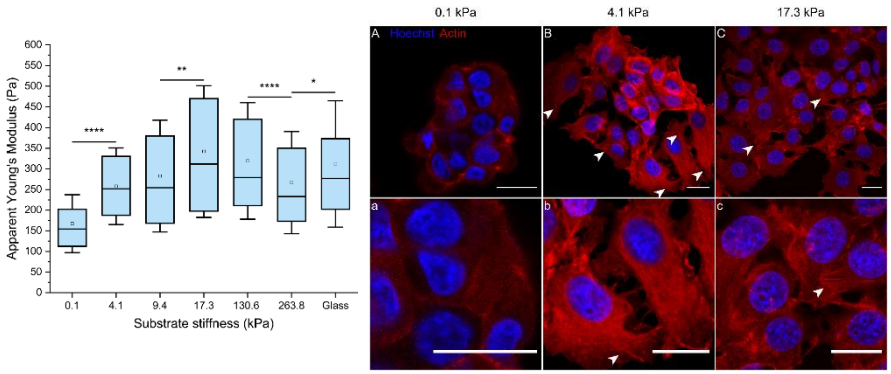

Left: Elasticity (apparent Young's modulus) of MCF-7 cells seeded on polyacrylamide gels of varying stiffness. Cell stiffness increase with substrate stiffness, reaching a maximum for cells seeded on 17.3 kPa gels.

Right: Confocal microscopy images of MCF-7 cells plated on three different gels. Actin cytoskeleton is shown in red, while nuclei are stained in blue. Cells seeded on stiffer gels show a spread morphology with a well-defined actin cytoskeleton, including marked actin stress fibers (indicated by white arrow heads). In contrast, cells plated on the softest gel show a rounded morphology and a diffuse actin labelling.

Temperature and hydrophobic forces determine the mechanical unfolding of a titin 27 polyprotein

Juan Carlos Gil-Redondo[1], Andreas Weber[1], Ulrich Fuchs[1], José L. Toca-Herrera[1]

[1]Institute of Biophysics, Department of Nanobiotechnology, University of Natural Resources and Life Science, Vienna, Austria

Objective

Protein function is dependent on its 3D structure. Any small changes in the homeostatic environment surrounding a protein can alter their structure, and therefore, their function. Different studies show that temperature has an effect on protein stability and flexibility. Several forces are stablished between the lateral chains of the aminoacids forming the polypeptide, such as van der Waals, hydrogen bonds, electrostatic and hydrophobic forces. This forces are responsible for the stability of the protein. Such stability has been usually tested through chemical or thermal denaturation. In the present work, we use atomic force microscopy (AFM) in single-molecule force spectroscopy (SMFS) experiments where we mechanically unfold a custom protein polymer containing nine copies of titin I27 domain, allowing for the characterization of the unfolding energy landscape. Force vs stretching curves show a sawtooth pattern where each peak corresponds to the unfolding of one I27 domain. Fitting a worm-like chain (WLC) model provides information about the changes in the contour length of the protein and the force required to unfold it. Unfolding of this polyprotein at different pulling speeds provides information about several kinetic parameters based on a two-state protein unfolding model which, in turn, allows us to determine changes in the stability and flexibility of the protein. Changing the temperature or altering the hydrophobic forces of the proteins after adding ethanol to the solution allowed us to analyze the importance of these parameters in this process.

Results & Conclusion

Effects of temperature and reduction of the hydrophobic forces on the unfolding kinetics of the protein are shown in the table. In summary, increasing temperature of the environment causes an increment on the distance to the transition state from the folded state of the protein (ΔX_u) without affecting the energy of the transition state barrier ($\Delta G^{\ddagger}$). On the other hand, decreasing hydrophobic forces with ethanol increases both ΔX_u and $\Delta G^{\ddagger}$. In both cases, a decrease in the spring constant of the protein (D) is observed, meaning that the protein becomes more flexible or malleable.

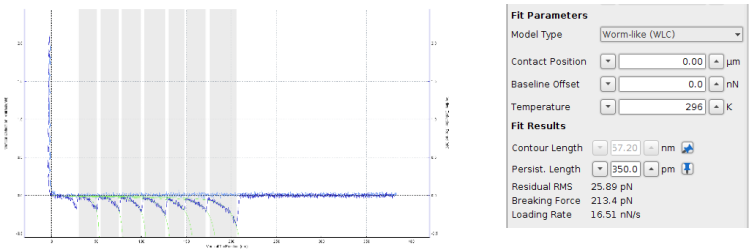

Experimental condition	ΔX_u		$\Delta G^{\ddagger}$	D
18 °C	0.130 nm		29.29 k_BT	13.83 N/m
Control (23 °C)	0.152 nm		30.54 k_BT	10.78 N/m
37 °C	0.165 nm		29.92 k_BT	9.35 N/m
30% EtOH (23 °C)	0.273 nm		38.23 k_BT	4.19 N/m

Top: example force curve of the unfolding of the polyprotein and WLC fitting.
Bottom: table showing the different kinetic parameters related to the protein unfolding.

Expression of a Titin I27 polyprotein and characterization of the mechanical unfolding with AFM

Ulrich Fuchs[1], Andreas Weber[1], José Luis Toca-Herrera[1]

[1]Institute of Biophysics, Department of Nanobiotechnology, University of Natural Resources and Life Science, Vienna, Austria

Objective

The three-dimensional structure of a protein is determined by the amino acid chain, and intramolecular interactions between the amino acids shape the energy landscape that a protein follows when folding. Generally, the native, folded state of a protein is thought to be the thermodynamically most stable state that the protein can be in. One way is to mechanically unfold a protein by application of a force using an Atomic Force Microscope. The objective of this work was to establish an expression routine for a Titin I27 polyprotein and characterise the mechaincal unfolding using AFM at different unloading rates. Finally, Bell-Evans theory was used to describe the unfolding kinetics.

Results & Conclusion

A polyprotein with 9 single Titin I27 domains was expressed successfully with a N-terminal His-tag and a C-terminal cysteine tag in E. coli. They were then purified with a Ni-based affinity chromatography step, and dialysed in PBS. For measurements, glass slides were coated with gold and the proteins were bound to the surface over a thiol bond. They were then measured by AFM using a force map approach with different unloading rates ranging from 200 nm/s up to 12.8 µm/s. A worm-like chain model was used to fit the data, and from these sets, the unfolding length and unfolding force was calculated.

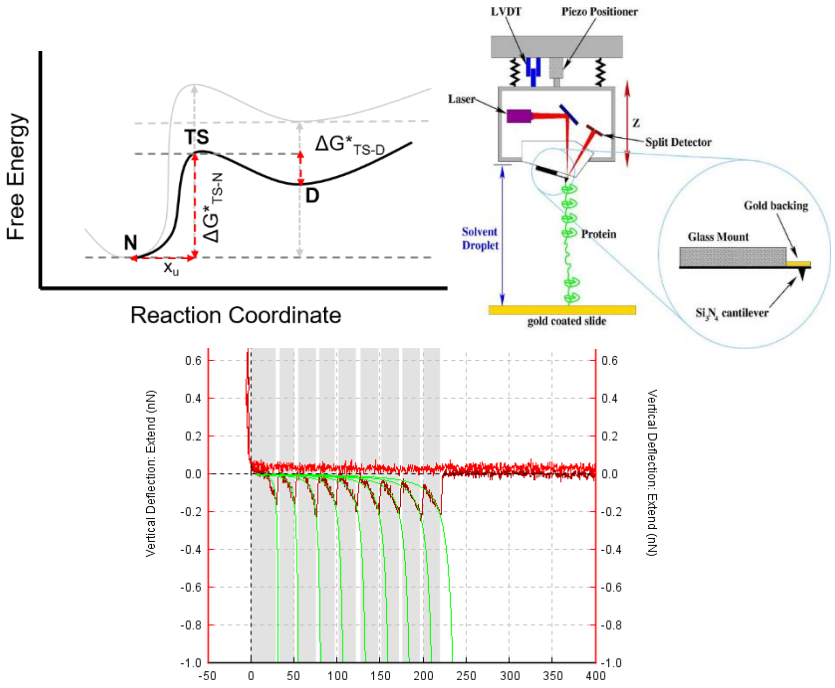

Figure: Energy landscape of unfolding (upper left). Schematic drawing of measurement setup (upper right). Representative curve and worm-like chain model fitting (bottom middle)

Expression of Titin I27 polyprotein and its mutants

Veronika Pavlovska[1], Amsatou Andorfer-Sarr[1], Andreas Weber[1], José Luis Toca-Herrera[1]

[1]Institute of Biophysics, Department of Nanobiotechnology, University of Natural Resources and Life Science, Vienna, Austria

Objective

Mechanical forces play important roles in biological systems. Some of these include roles in tissue formation, embryogenesis, movement and many more. On the smallest scale, these forces are transduced by proteins through conformational changes. Therefore, it is important to study the mechanical unfolding behaviour of proteins. This will help to gain new insights into the physical basis of protein folding and unfolding, as well as misfolding in disease. In this project, a de novo synthesis of I27 octameric polyproteins was performed with focus on molecular biology. The next step is then to introduce single amino acid mutations by site-directed mutagenesis.

Results & Conclusion

For the present project, a multiplicative cloning approach was performed, as the repetitive nature of the plasmid makes it impossible to perform just a single step cloning. The approach can be seen in the Figure below. First, a restriction step was performed, followed by insertion of a ligated insert, this step was repeated 3 times. The lower figure shows a gel electrophoresis result of a successfully produced 4x I27 plasmid. The final 4+4 step is not yet working.

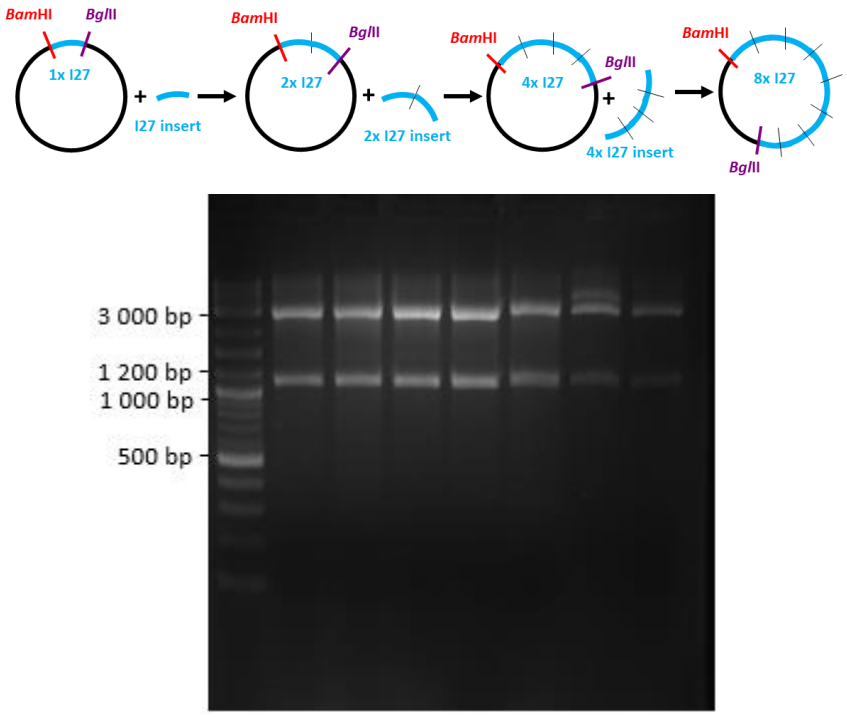

Figure: (Top) Multiplicative cloning approach. (Bottom) Gel electrophoresis of a successfully produced 4x Titin I27 plasmid.

A-to-I RNA editing of Filamin A (FLNA) regulates cellular adhesion, migration and mechanical properties

Andreas Weber[2], Mamta Jain[1], Greeshma Manjaly[1], Joanna Deek[3], Olena Tsvyetkova[1], Maja Stulić[1], Andreas Bausch[3], José L Toca-Herrera[2], Michael F. Jantsch[1]

[1]Division of Cell Biology, Center of Anatomy and Cell Biology, Medical University of Vienna, Austria
[2]Institute of Biophysics, Department of Nanobiotechnology, University of Natural Resources and Life Science, Vienna, Austria
[3]Cellular Biophysics E27, Department of Physics, Technical University of Munich, Germany

Objective

A-to-I RNA-editing by ADARs is an abundant epitranscriptomic RNA-modification in metazoa. Flna pre-mRNA in mammals harbors a single conserved A-to-I RNA editing site that introduces a Q-R amino acid change in Ig-repeat 22 of Rod2 domain of the encoded protein. Previously, we showed that FLNA editing regulates smooth muscle contraction in the cardiovascular system and cardiac health. The present study investigates how ADAR2-mediated A-to-I RNA editing of Flna affects actin crosslinking, cell mechanics, cellular adhesion and cell migration.

Results & Conclusion

Cellular assays and AFM measurements demonstrate that the edited version of FLNA increases cellular stiffness and adhesion but impairs cell migration in both mouse fibroblasts and human tumor cells. In vitro, edited FLNA leads to increased actin crosslinking forming actin gels of higher stress resistance. Our study shows that Flna RNA editing is a novel regulator of cytoskeletal organization, mechanical propertiesy of cells and mechanotransduction.

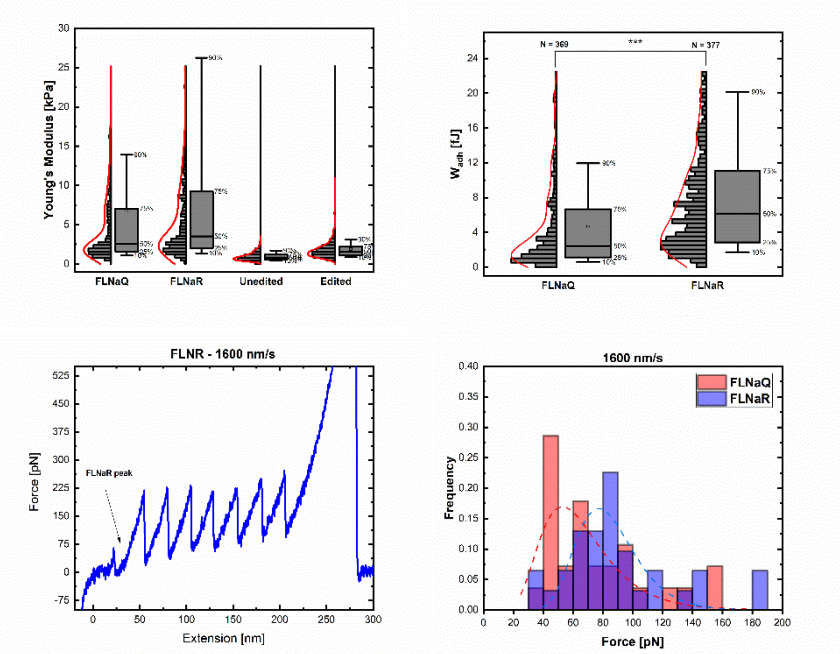

Figure: (**Top Left**) Comparison of cellular elasticity for cells with and without single amino acid mutation of FLNa. (**Top Right**) Comparison of adhesive work between AFM cantilever and cell surface of mouse rat fibroblasts with and without the mutation. (**Left Bottom**) Representative curve of protein unfolding of a single domain of the FLNa protein inserted into a Titin I27 structure. (**Right Bottom**) Comparison of unfolding forces for the different protein variants at 1600 nm/s.

Using Machine Learning Approaches to Classify AFM Force Spectroscopy Curves

Victoria Beneder[1], Tobias Eder[1], Andreas Weber[1], Rafael Benitez[2], José Luis Toca-Herrera[1]

[1]Institute of Biophysics, Department of Nanobiotechnology, University of Natural Resources and Life Science, Vienna, Austria
[2]Department of Business Mathematics, University of Valencia, Spain

Objective

In Force Spectroscopy methods, the AFM cantilever is used as an indentation device and the deformation of the sample is recorded at a given force threshold and over a certain time. This enables the study of mechanical properties and their dependence of time and frequency. As biological materials are complex, hierarchical, multistructured objects, often one needs to perform a high number of experiments to ensure sampling of the statistical distribution. Here we set out to use different machine learning algorithms to distinguish between curves that are deemed "good" and "bad" for later computational analysis. This simple classification is often needed, as sample properties can change over time, measurements in liquid are prone to errors, and other sources of noise (e.g. electrical noise, vibrations of the building, acoustics) can lead to curves with shapes that make later automatic computational processing very complex.

Results & Conclusion

Force Spectroscopy curves were recorded either on glass, cells, or hydrogels. The medium was either air or measurement buffer. Different sources of noise were artificially created to produce errors in measurements on purpose. Then curves were classified by hand in "good" and "bad", and different machine learning algorithms (random forest, logistic regression, support vector machine) were trained. These were then used to classify datasets, and excellent matching rates were achieved. To reduce processing time, a curvature-based sampling method was additionally developed.

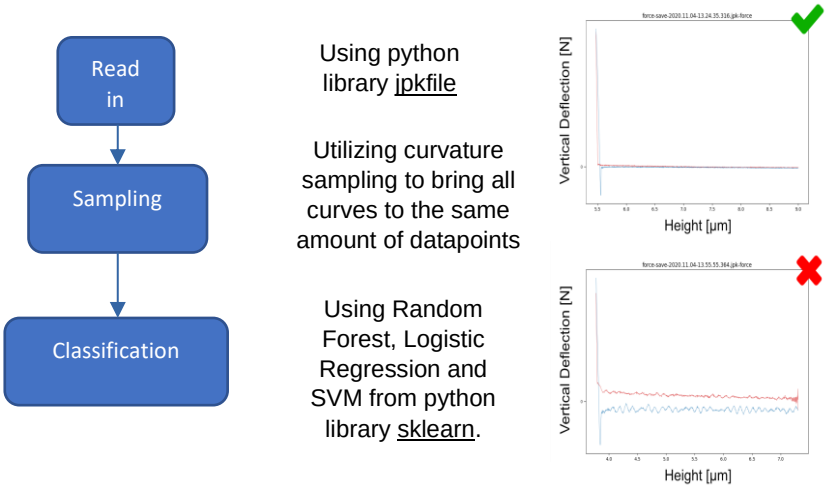

Figure: Routine of curve processing steps for classification algorithm.

Automatic Detection of Protein Unfolding Events in AFM studies

Victoria Beneder[1], Tobias Eder[1], Andreas Weber[1], Ulrich Fuchs[1], Rafael Benitez[2], José Luis Toca-Herrera[1]

[1]Institute of Biophysics, Department of Nanobiotechnology, University of Natural Resources and Life Science, Vienna, Austria
[2]Department of Business Mathematics, University of Valencia, Spain

Objective

Unfolding proteins by application of a mechanical force is a today widely used method to study the energetics and kinetics of the protein folding problem. For this purpose, polyproteins of defined domain sequences are produced and then mechanically stretched with an AFM. This single molecule method has multiple positive compared to ensemble methods (as e.g. spectroscopic studies), but thousands of unfolding curves need to be measured to ensure sampling of the statistical distribution. Classically, these then must be classified (in curves with and without events), processed (baseline corrections, noise corrections, determination of CP and DP, removal of cantilever bending) and fitted with polymer elasticity models (e.g. worm-like chain). The aim of this project is to program an algorithm that automatically performs the processing and fitting steps.

Results & Conclusion

A nine repeat Titin I27 polyprotein was mechanically unfolded by AFM with loading rates ranging from 400 nm/s to 12.8 µm/s. A modified version of the jpkfile Python library was used to read in curves and they were pre-processed using a Python conversion of the in-house built R package RafmToolkit. Then, curves were smoothed applying a fast fourier transform (with optimized cut-off frequencies), and a Mexican hat wavelet algorithm was used for peak detection. These were then fitted individually applying a least squares fitting of a worm-like-chain model.

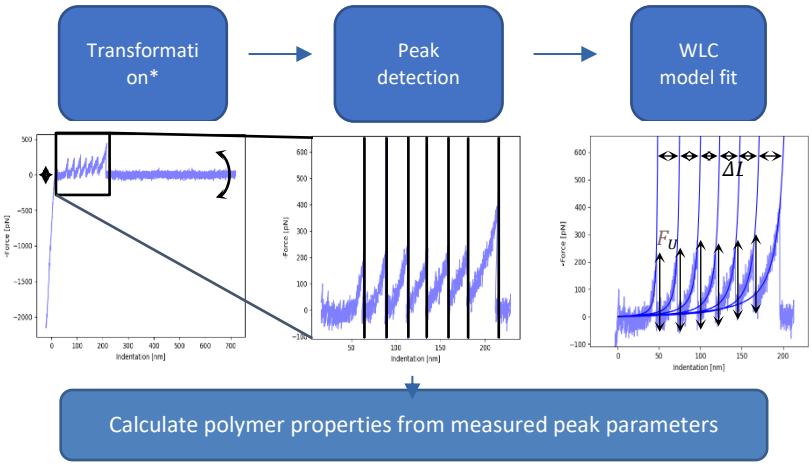

Figure: Routine of curve processing steps for protein unfolding peak detection algorithm.

Automatic Detection of Tethers and other Adhesion Events in Retraction Curves

Tobias Eder[1], Victoria Beneder[1], Andreas Weber[1], Rafael Benitez[2], José Luis Toca-Herrera[1]

[1]Institute of Biophysics, Department of Nanobiotechnology, University of Natural Resources and Life Science, Vienna, Austria
[2]Department of Business Mathematics, University of Valencia, Spain

Objective

Cellular adhesion is a complex process involving different types of specific and unspecific interactions. One way to probe cell adhesion is the use of Atomic Force Microscopy, where a sample is first indented with the probe and the cantilever is bend towards the sample when retracting because of attractive adhesive interactions. In similar fashion, one can perform similar measurement using a cell as a probe, therefore enabling the measurement of cell-cell and cell-substrate interaction. The adhesion pattern is a mixture of mechanical (viscous and plastic deformation) and molecular elasticity (tether formation, protein unfolding, homo and heterotypic protein interactions) features. With respect to the latter, they can be found up to tens of µm away from the cell surface and the related force steps are in the range of tens of pN. Therefore, automatic detection of such events in retraction curves is not an easy task. Here we provide a novel algorithm to detect tethers and and other events in the adhesion segments of force distance curves.

Results & Conclusion

Force distance curves were performed with spherical indenters on MCF-7 and MCF-10a breast cancer cells. The curves were downsampled using a curvature based algorithm and then transformed with the AFM toolkit. Then a FFT was done to remove high frequency noise and the first derivate was calculated. Peak detection was done by thresholding and prominence. Finally, slopes were fitted to 500 nm before the events and they were classified as tethers (0 +/- 10 pN/µm) or other events. Then, event properties (position, length, work, force, slope, number) were determined.

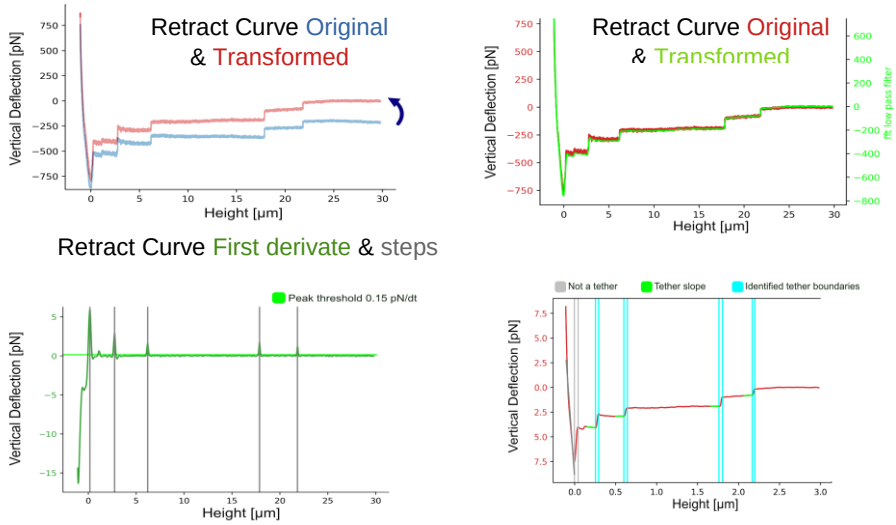

Figure: *Routine of curve processing steps for tether event detection algorithm*

Viscoelastic Properties of Eukaryotic Cells Measured with AFM

Andreas Weber[1], Rafael Benitez[2], José Luis Toca-Herrera[1]

[1]Institute of Biophysics, Department of Nanobiotechnology, University of Natural Resources and Life Science, Vienna, Austria
[2]Department of Business Mathematics, University of Valencia, Spain

Objective

Cells are viscoelastic bodies and show time and frequency dependent mechanical properties. They are complex, multi-layered, hierarchical, living systems. The interplay and coupling between cytoskeletal elements, cross-liners, adhesion sites, the nucleus and the membrane defines their mechanical properties. In literature, two major branches of viscoelastic models are often used to fit cell mechanical measurements: constitute linear viscoelastic models and fractional (power law) models. Here, different sets of models were applied to describe the mechanical properties of cells under stress relaxation conditions.

Results & Conclusion

Hela cells were measured with AFM using a spherical indenter with defined stress relaxation segments (1, 10 and 60 s pause with force setpoints of 0.5, 1, 2, 4 and 8 nN). A power law model, a standard linear solid and a five-element Maxwell model were used to fit the stress relaxation segment.

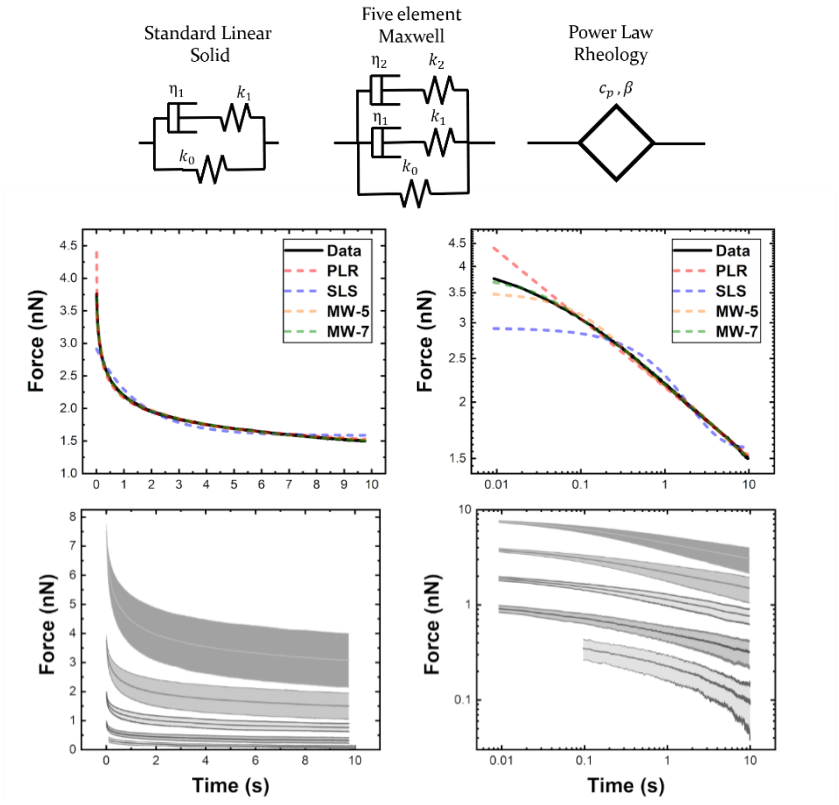

Figure: (**Top**) Description of the three different models used for the analysis. (**Middle**) Fitting of 4 nN 10 s curves with four different models, either in normal or logarithmic view. (**Bottom**) Averaged force-time-curves for 10 second pause segments.

For fitting purposes, the R afmToolkit was used. Curves were imported and corrected (contact point, detachment point, baseline correction, cantilever bending correction). Then, the Force-time trace was fitted either with a decaying power law, or a single or double exponential decay function. To

determine mechanical properties, the hereditary Boltzmann integral connecting stress to strain was solved for stress relaxation conditions. In addition, a substrate correction factor was applied.

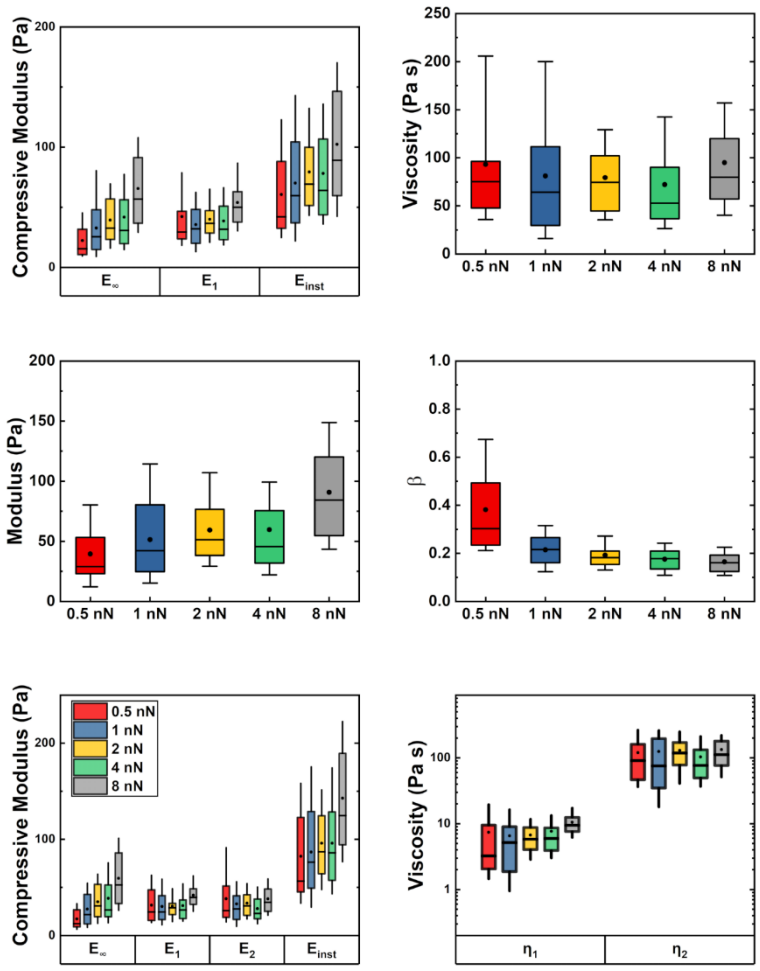

Figure: Boxplots of the evaluation using three different models (SLS top, PLR middle and five element Maxwell model bottom) for measurements performed over 10 s. The boxplots show the median (line), the mean (dot), range from the 25th to the 75th percentile and the whisker range from the 10th to the 90th percentile.

Apparently, the measured modulus is significantly higher when using a force of 8 nN compared to all other (applied) forces. Interestingly, regarding the viscosities, no dependence on the load (and therefore indentation depth) can be seen. Furthermore, for measurements performed with 0.5 nN step load, a lower modulus was found. Regarding the power law approach, an inverse scaling of the power law exponent was apparent (which is closer to zero for elastic solids and closer to the one for a viscous fluid). With respect to fitting quality, the standard linear solid performed not as well (R^2 of around 0.7 to 0.8) as the power law and the five element Maxwell model (R^2 consistently between 0.95 to 0.99). Note that for this analysis the residual distribution was used and found to be normally distributed, enabling the R^2 value as approximation of goodness of fit. Comparing the ratio of the time-scales of relaxations with the experimental scales (Deborah number), leads to the conclusion that the Deborah number remains conserved.

Modelling cell fluidisation after actin depolymerisation using AFM Stress Relaxation experiments

Andreas Weber[1], Rafael Benitez[2], José Luis Toca-Herrera[1]

[1]Institute of Biophysics, Department of Nanobiotechnology, University of Natural Resources and Life Science, Vienna, Austria
[2]Department of Business Mathematics, University of Valencia, Spain

Objective

The viscoelastic properties of eukaryotic cells are defined by their constituents. Of these, the different cytoskeletal elements – actin filaments, microtubules and intermediate filaments – are the ones that mostly contribute. In literature, actin filaments and the actin cortex are deemed to be the most important elements determining cellular stiffness, viscosity and active cell mechanics. A simple way to study the importance of the different structures is to modify them by chemical agents. In this study, actin filaments of Hela cells were depolymerized chemically using Cytochalasin D and then cells were subjected to stress relaxation measurements for 10 s using AFM.

Results & Conclusion

A standard linear solid, five-element Maxwell and power law rheology model were used to fit the data-sets. The curve shape appeared similar to control curves, with the difference that relaxation times appeared shorter and the overall relaxation appeared higher, hinting towards cells becoming softer and more fluid.

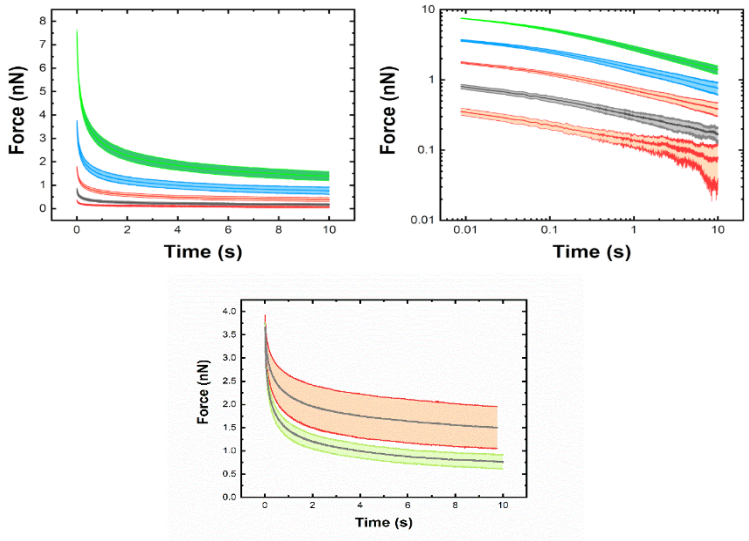

Figure: (**Top row**) Force time and logarithmic view of 10 s stress relaxation curves performed on CytoD-treated Hela cells. (**Bottom**) Comparison of averaged curve (+/- standard deviation) for control (reddish) and CytoD treated cells (green).

	Control					CytoD				
F [nN]	0.5	1	2	4	8	0.5	1	2	4	8
τ_1	0.18	0.18	0.20	0.24	0.23	0.07	0.12	0.16	0.18	0.18
τ_2	3.51	3.51	3.35	3.50	3.05	3.03	2.15	2.49	2.56	2.46

Table 1: Comparison of relaxation times (in s) for control and CytoD treated Hela cells using a five element Maxwell model.

	Control					CytoD				
F	0.5	1	2	4	8	0.5	1	2	4	8
E	39	51	59	60	91	18	25	25	30	39
β	0.38	0.21	0.19	0.18	0.16	0.39	0.29	0.27	0.27	0.29

Table 2: Comparison of power law rheology model for control and CytoD treated Hela cells using 10 second relaxation time curves. Force is given in nN.

	Control					CytoD				
F	0.5	1	2	4	8	0.5	1	2	4	8
E_∞	17	27	35	39	59	15	14	14	16	20
E_1	32	30	30	31	42	32	33	29	35	50
E_2	38	33	34	28	38	19	23	18	22	30
η_1	7	7	7	8	11	4	4	5	6	9
η_2	120	125	130	103	134	43	44	47	56	74

Table 3: Comparison of fitting results gained for either Control or CytoD-treated cells using a five element Maxwell model with measurement times of 10 s. Force is given in nN.

Can we use power laws to describe the mechanical properties of bacteria?

Andreas Weber[1], José Luis Toca-Herrera[1]

[1]Institute of Biophysics, Department of Nanobiotechnology, University of Natural Resources and Life Science, Vienna, Austria

Objective

In this chapter, novel data regarding the mechanical properties of bacterial cells (E. coli as model organism) is presented. The cell envelope is the main structure determining bacterial cell shape and their resistance to external influences, is counteracting the bacterial turgor pressure and is important for intra- and extracellular transport. As bacterial cells are one of the most often used expression system in industrial recombinant protein production, their shape and stability as response to stresses induced by protein production are an interesting subject of studies.

Bacteria were first immobilized making use of electrostatic interactions, then low resolution AFM images were performed which was needed for identifying the position of bacteria. This was followed by employing Force-Volume mode to determine with spatial resolution the elastic properties of the cells. For investigation of the viscoelastic properties, measurements at different loading rates ranging from 0.25 to 128 µm/s were performed.

Results & Conclusion

To characterize the mechanical properties of bacteria, a nanometric AFM tip was used and 20 nm of the indentation curve were fitted by a Hertzian mechanical model with Sneddon extension. The Figure below shows a phase contrast microscopy image with an overlay of height images of bacterial individual cells performed in QI mode.

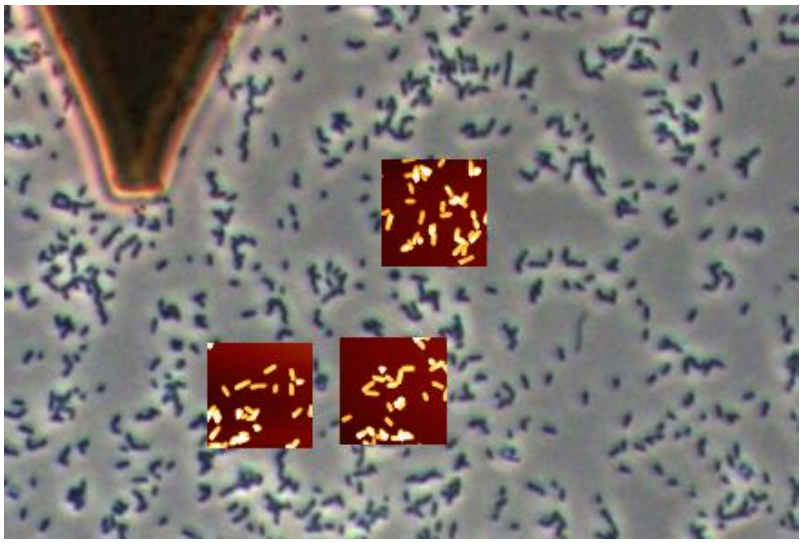

Figure 1: Phase contrast microscopy image (EC "Plan-Neofluar" 10x/0.3) with inset of 20x20 µm QI mode height images. The cantilever shape can be seen on the top left of the image.

In a next step, higher resolution force mapping was performed and for each pixel the Young's Modulus was evaluated. This revealed that the apparent Young's Modulus (using a pyramidal indentation shape) is in the range of MPa and constant over the central region of the bacterial cell.

This fits together well with what is already published in literature. Such an analysis can be seen in the Figure below. To identify necessary statistics (how many measurements per cell and how many cells), this analysis was performed for 50 bacterial cells.

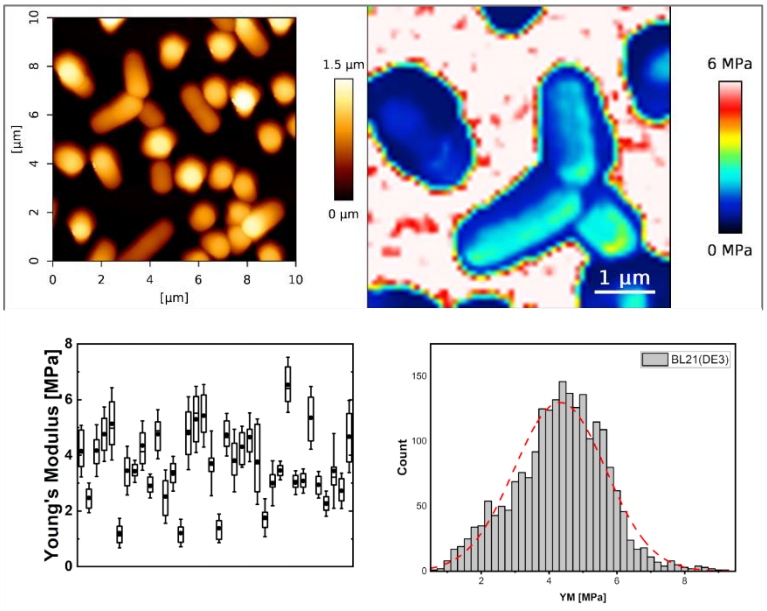

Figure: (Top row): QI image (10 x 10 µm, 128 x 128 pixels) with Young's Modulus mapping as an inset (10 µm/s, 128 x 128 pixels). (Bottom row) Analysis of statistical distribution.

Indentation experiments were performed using loading rates ranging from 0.25 to 128 µm/s and then fitted using either the pyramidal or the parabolic contact geometry. The dependence of the calculated apparent modulus was well fitted using a weak power law model $E(\omega) = E_0 \left(\frac{\omega}{\omega_0}\right)^{\alpha}$. This analysis and the parameters of the fitting can be seen below.

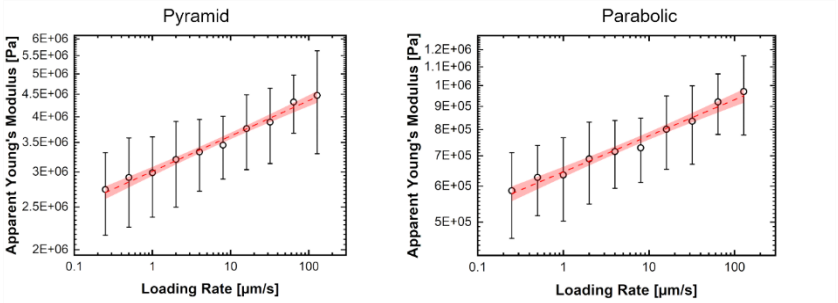

Figure: Power law rheological fitting of Young's Modulus dependence of bacterial cell mechanics. (Left) Fittings using the pyramidal geometry were performed. (Right) Parabolic geometry was used to fit the data. The fitting corresponds to a simple Power Law Model and the red area is the 5% confidence interval of the fitting.

Table: Fitting results for a power law model applied to the loading rate dependent mechanical properties of bacteria.

Model	E_0 [MPa]	β	R^2
Pyramidal	3.009 ± 0.003	0.080 ± 0.003	0.98
Parabolic	0.645 ± 0.001	0.079 ± 0.004	0.97

Viscoelasticity of bacterial cells measured by AFM creep experiments

Andreas Weber[1], José Luis Toca-Herrera[1]

[1]Institute of Biophysics, Department of Nanobiotechnology, University of Natural Resources and Life Science, Vienna, Austria

Objective

Today still, only few studies have been concerned with measuring the mechanical properties of bacteria, using mostly elastic theories to model the measured data. With respect to viscoelastic models, a simple standard linear solid model is sometimes used. The main component determining the mechanical properties of bacteria (in this case gram-negative E. coli) is the cell wall, consisting of the inner membrane, a thin peptidoglycan layer and the outer membrane. Creep measurements were done to revisit the viscoelastic properties of the bacteria. As a novelty, I will introduce power law rheology to model the measured mechanical properties.

Results & Conclusion

E. coli were immobilized on PEI coated glass slides and imaged by AFM using the QI mode. Then, they were measured under creep conditions, following the increase of deformation over time when keeping the applied stress constant. The creep function of a viscoelastic material is defined as monotonically increasing and is described by the hereditary Boltzmann integral. Here a solution for standard linear solid following $Z(t) = \frac{F_0}{k_0} + \frac{F_0}{k_1}\left(1 - e^{-t\frac{k_1}{\eta_1}}\right)$ and a solution using a power law model following $Z(t) = \frac{F_0}{k_0}\left(\frac{t}{t_0}\right)^{\beta}$ was used. The figure below shows an array of randomly chosen creep curves (16x16 curves on the middle region of the cells were measured).

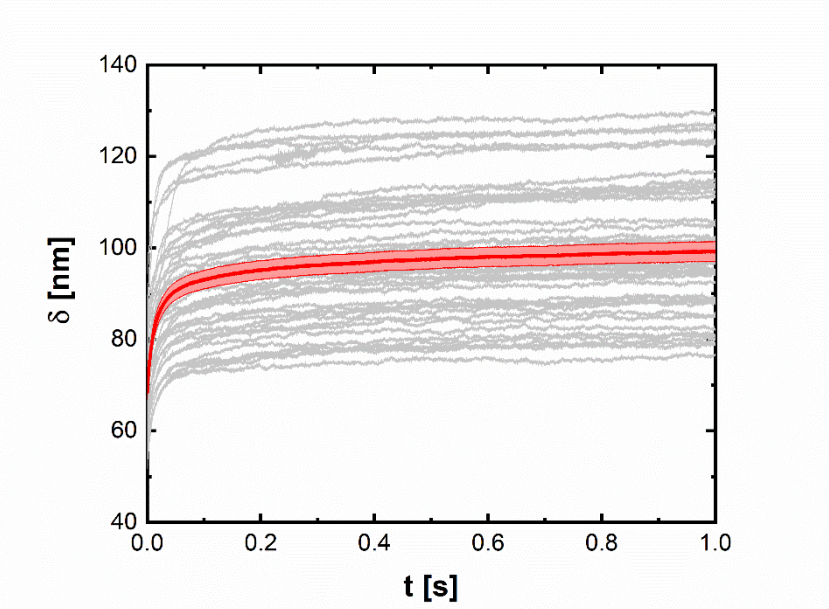

Figure 1: Creep curves (indentation vs. time) at 1 nN measured with a pyramidal tip for 1 s. The grey curves are 30 measurements taken randomly from a 16 x 16 force map, while the red line corresponds to the average of all measurements and the standard error of averaging (width around the central line).

The shape of the indentation-time curves appears similar to what is already published in literature. Therefore, the three above described models were fitted to the data. Such an analysis can be seen in the figure below.

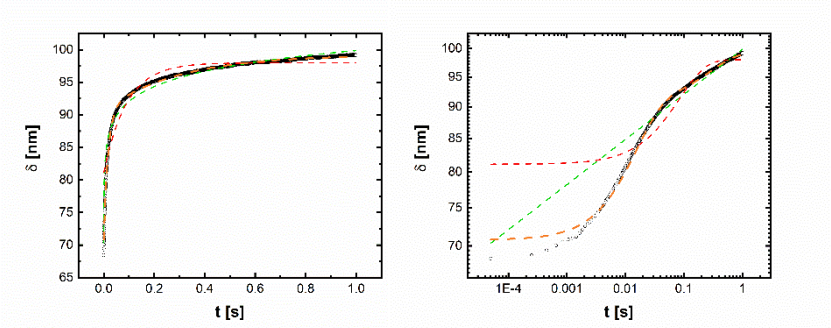

Figure 2: Fitting of SLS or PLR model to creep data. Left shows the curves as indentation vs time, while the right side shows them in the logarithmic scales. In red the SLS is shown while in green the PLR is shown and in orange the 5-element Maxwell model can be seen.

As already widely discussed in literature, a PLR model is better in fitting at the smaller and longer time scales, while an exponential model fits well the intermediate ones (1 to 10 s). What can be seen is that the creep phase is apparently not fully completed after 1 s, indicating that longer pause times are needed for the measurements. The model that best fits the data set is the 5-element Maxwell model. The table below shows the calculated statistical properties for the power law and the standard linear solid model.

Table: Fitting results for the viscoelastic models that were applied to the creep segments of the curves. The error shown is the standard error.

Model	k_0 [N/m]	k_1 [N/m]	τ [s]	β	R^2
SLS	0.013 ± 0.002	0.061 ± 0.017	0.103 ± 0.068	n.a.	0.885
PLR	0.010 ± 0.001	n.a.	n.a.	0.035 ± 0.008	0.906

Power laws in eukaryotic cell mechanics based on AFM measurements

Andreas Weber[1], Barbara Zbiral[1], Rafael Benitez[2], José Luis Toca-Herrera[1]

[1]Institute of Biophysics, Department of Nanobiotechnology, University of Natural Resources and Life Science, Vienna, Austria
[2]Department of Business Mathematics, University of Valencia, Spain

Objective

AFM is probably the most often used technique in investigating cell mechanics, since it allows for measuring the interaction of matter with matter under ambient conditions, with a wide variety of measurement conditions, indenter geometries, functionalized tips. Eukaryotic cells (and in our case mammalian cells) are a fascinating example of complex hierarchical materials, with a size in the range of tens of µm. Here we will test the applicability of simply Hertzian mechanical models to describe the dependence of measured mechanical properties of the measurement frequency.

Results & Conclusion

The model is applied to simple force-cycles (indenting the cell and then removing the pressure). Two different geometries are tested: First, nanometric four-sided pyramidal tips are used and then spherical particles of different sizes (2, 5, 10 and 20 µm diameter). As discussed above, tips lead to strictly localized, high pressure, while using particles, one measures the response of the whole cell. The frequency range examined in this study ranges from 0.5 to 100 Hz while the force range used is 0.1 to 10 nN for tip measurements and 1 to 25 nN for particles, respectively. The different used indenter geometries can be seen in the figure below. The table below summarizes the measurement settings.

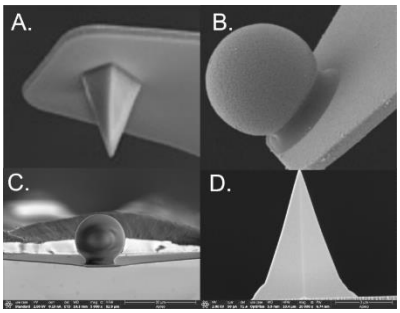

Figure: SEM micrographs of particles and cantilevers used in this study. (A) DNP-S tip (taken from manufacturer website). (B) CP-PNPL-SiO-A5 tip (from manufacturer website). (C) 20 µm particle glued to NP-O cantilever. (D) DNP-S tip side-view.

	Settings tip	Settings particles
Loading rate [µm/s]	0.5, 2, 5, 10, 20	0.1, 0.5, 1, 2.5, 5, 10, 25, 50
Load [nN]	0.1, 0.5, 1, 2.5, 5, 10	1, 2.5, 5, 10, 17.5, 25

Table: Measurement settings employed to test frequency dependence.

For data evaluation, curves were pooled and the R afmToolkit was used. The figure below shows the averaged force distance curves using the different particle sizes and a load of 2.5 nN. It can be seen that the indentation is inversely proportional to the used loading rate.

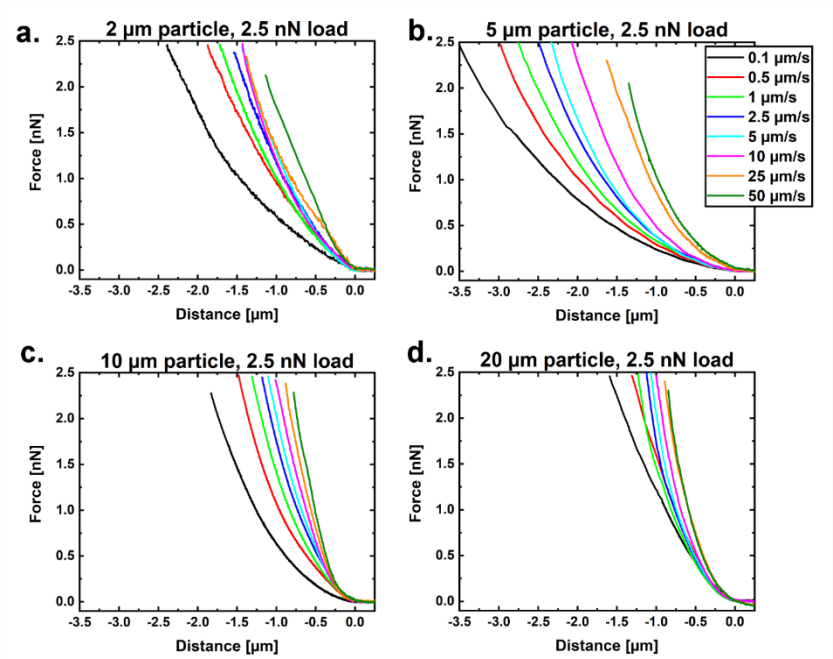

Figure: Averaged force distance curves for maximum load of for varying loading rates. (A) Measurements performed with a 2 µm particle and a load of 2.5 nN, (B) measurements performed with a 5 µm particle and a load of 2.5 nN, (C) measurements performed with a 10 µm particle and a load of 2.5 nN and (D) measurements performed with a 20 µm particle and 2.5 nN load.

In a next step, the apparent Young's Modulus was calculated for the different measurement settings using Hertzian mechanics with Sneddon extension. As an increase of this value could be seen with frequency, this relation was plotted and fitting following a power law as $E(\omega) = E_0 \left(\frac{\omega}{\omega_0}\right)^{\alpha}$. This analysis can be seen below.

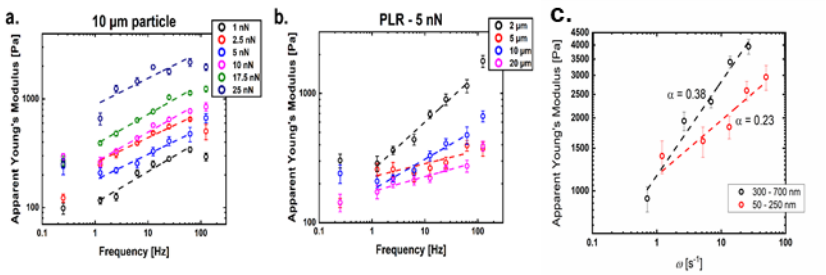

Figure: Analyis of power law dependence on frequency. (A) measurements for the 10 µm diameter particle with different force setpoints. (B) Comparison of power law behaviour for different particle sizes. (C) Comparison of power law behaviour using a pyramidal tip and different indentation ranges.

Frequency dependence of the mechanical properties of different biological materials

Lukas Krismer[1], Andreas Weber[1], José Luis Toca-Herrera[1]

[1]Institute of Biophysics, Department of Nanobiotechnology, University of Natural Resources and Life Science, Vienna, Austria

Objective

Biological materials show viscoelastic properties and often power laws can be used to describe the dependence of the measured apparent elastic modulus on the frequency. Here we set out to compare the mechanical properties of three different prevalent classes of biological materials (hydrogels, bacteria, eukaryotic cells). We applied AFM measured at loading rates ranging from 200 nm/s up to 64 µm/s. For the first case of material, different agarose gels (0.5 and 1.5% w/v) were prepared and measured with a spherical indenter. For the bacteria, E. coli (BL21 DE3) were immobilized on PEI coated glass slides and measured with a nanometric pyramidal indenter. For cells, a 5 µm radius spherical particle was used to measure the mechanical properties of MCF-7 breast cancer cells.

Results & Conclusion

The two used hydrogels had average apparent Young's Moduli of 6 kPa (0.5% w/v) and 29 kPa (1.5%). The did not show any dependence on the loading rate. The studied E. coli had moduli in the range of 1 MPa, which depended slightly on the loading rate. Finally, the breast cancer cells were the softest of the materials studied, with Young's Modulus ranging from 150 Pa for the slowest measurements up to 600 Pa for the fastest. The figure below shows an analysis of a power law used to describe these relationships.

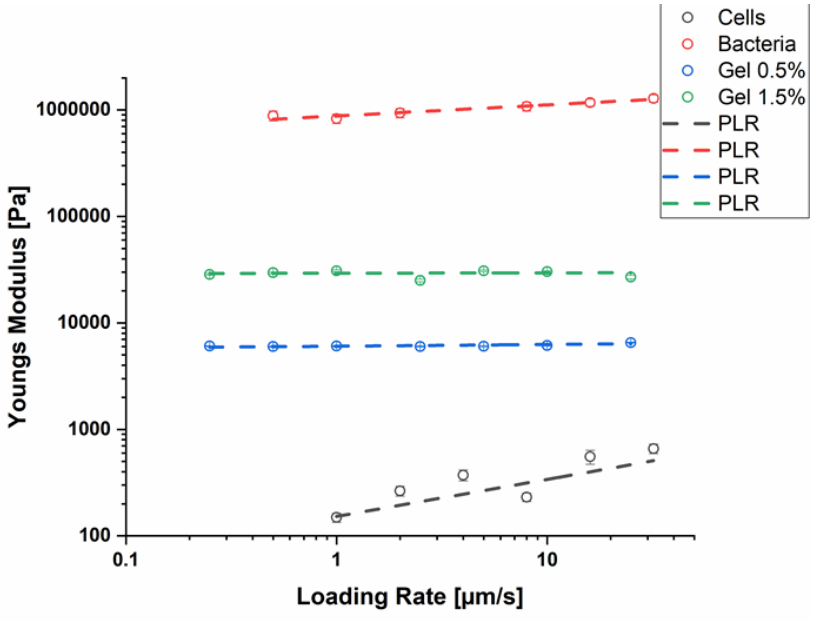

Figure: Power Law Rheology analysis of all studied materials. The dashed line indicates the power law fitting while the open circles indicate the Young's Modulus values and the error shown is the standard error.

Estrogen Modulates Epithelial Breast Cancer Cell Mechanics and Cell-to-Cell Contacts

Andreas Weber[1], Barbara Zbiral[1], Maria dM Vivanco[2], José Luis Toca-Herrera[1]

[1]Institute of Biophysics, Department of Nanobiotechnology, University of Natural Resources and Life Science, Vienna, Austria
[2]Cancer Heterogeneity Lab, CIC bioGUNE, Bizkaia Science and Technology Park, Derio, Spain

Objective

Excessive estrogen exposure is connected with increased risk of breast cancer and has been shown to promote epithelial-mesenchymal-transition. Malignant cancer cells accumulate changes in cell mechanical and biochemical properties, often leading to cell softening. In this work we have employed atomic force microscopy to probe the influence of estrogen on the viscoelastic properties of MCF-7 breast cancer cells cultured either in normal or hormone free-medium.

Results & Conclusion

Estrogen led to a significant softening of the cells in all studied cases, while growing cells in hormone free medium led to an increase in the studied elastic and viscoelastic moduli. In addition, fluorescence microscopy shows that E-cadherin distribution is changed in cells when culturing them under estrogenic conditions. Furthermore, cell-cell contacts seemed to be weakened. These results were supported by AFM imaging showing changes in surfaces roughness, cell-cell contacts and cell height as result of estrogen treatment.

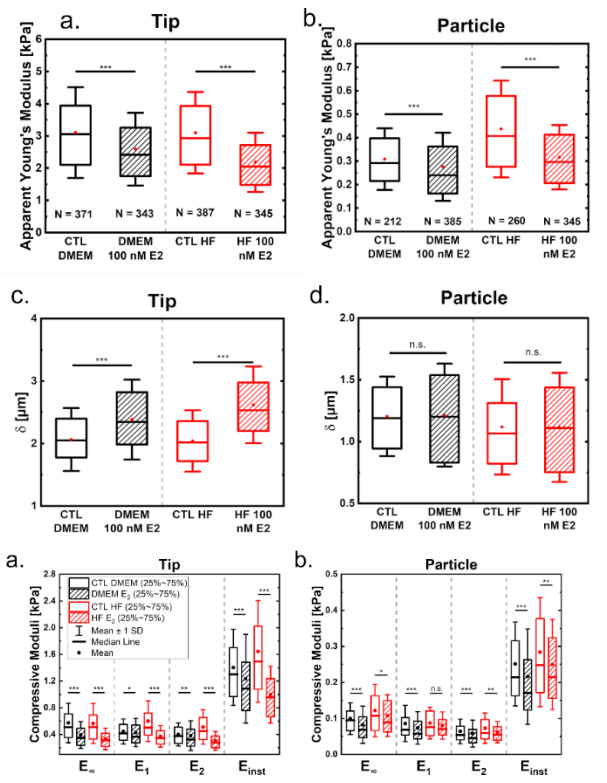

Figure: Mechanical properties of MCF-7 breast cancer cells depend on the estrogen level of the culture medium. (Top row) Elastic Modulus measured with tip (left) or particle (right). (Middle row) Indentation measured with tip (left) or particle (right). (Bottom row) Viscoelastic properties using a 5-element Maxwell model with a tip (left) or a particle (right).

This study therefore provides further evidence for the role of estrogen signaling in breast cancer.

Table: Median values of the elastic and viscoelastic properties derived for measurements on MCF-7 cells with either tips or particles (CTL and estrogen-treated).

	Tip				Particle			
	CTL DMEM	DMEM E_2	CTL HF	HF E_2	CTL DMEM	DMEM E_2	CTL HF	HF E_2
$E_{elastic}$ (Pa)	3058.9	2410.5	2933.1	2046.8	308.7	275.9	436.7	316.6
E_∞ (Pa)	507.9	347.9	508.8	312.7	94.5	68.4	107.5	89.3
E_1 (Pa)	416.2	364.7	501.0	347.8	68.0	57.3	75.9	69.9
E_2 (Pa)	374.9	321.6	449.3	277.2	53.7	45.3	59.6	55.0
E_{inst} (Pa)	1299.1	1085.3	1492.3	952.3	214.0	170.2	247.5	214.1
η_1 (Pa s)	71.2	69.05	81.8	65.8	12.0	10.2	14.1	11.8
η_2 (Pa s)	1067.7	912.5	1205.9	791.3	180.7	141.2	191.6	159.9

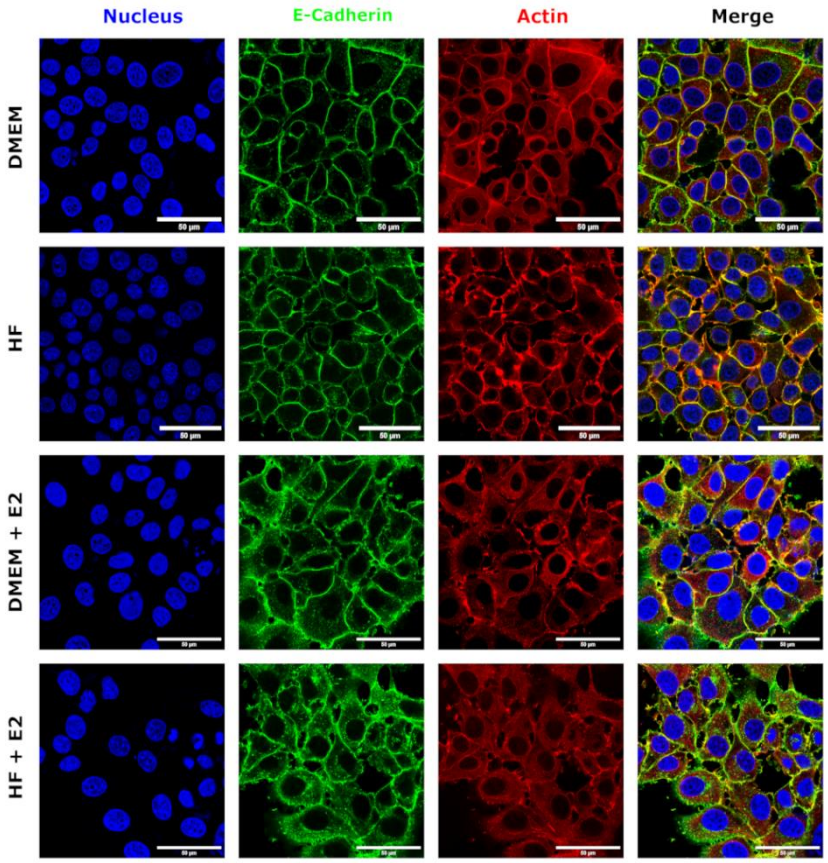

Figure: Confocal fluorescence microscopy images of MCF-7 cells grown either in DMEM, HF, DMEM supplemented with 100 nM estrogen or hormone-free medium enhanced with 100 nM estrogen. Nuclei are shown in blue, E-cadherin in green, actin in red. The scale bar corresponds to 50 µm.

Estrogen receptor interacting drugs and mechanical properties of epithelial breast cancer cells

Andreas Weber[1], Barbara Zbiral[1], Maria dM Vivanco[2], José Luis Toca-Herrera[1]

[1]Institute of Biophysics, Department of Nanobiotechnology, University of Natural Resources and Life Science, Vienna, Austria
[2]Cancer Heterogeneity Lab, CIC bioGUNE, Bizkaia Science and Technology Park, Derio, Spain

Objective

One of the most often published results in cell mechanics is that cancer cells appear softer than their healthy counterparts. This change is conserved over most tissues such as breast, bladder, colon or prostate cancer and the more aggressive cell lines are, the softer they appear. ER-positive breast tumours are generally considered less aggressive and have a better prognosis, but they can still develop resistance to drugs and become metastatic. ER-α is a nuclear transcription factor and known to be part of signaling cascades via genomic and non-genomic gen-expression regulation. Modulation of the receptor is often used as therapeutic approach in different pathological conditions. Some of these signaling events are connected to cytoskeleton remodeling, such as for actin filaments, microtubules and intermediate filaments. In this project, the role of estrogen receptor agonists and antagonists has been studied.

Results & Conclusion

AFM indentation curves were evaluated using a simple Hertzian elastic mechanics model. For indentation, a pyramidal tip was used and 500 nm of the indentation curve were investigated. The figure below shows the determined values and the overall indentation at a force of 1 nN. It is evident, that estrogen leads to a softening of cells, well the selective estrogen receptor modulators resveratrol and tamoxifen lead to a stiffening.

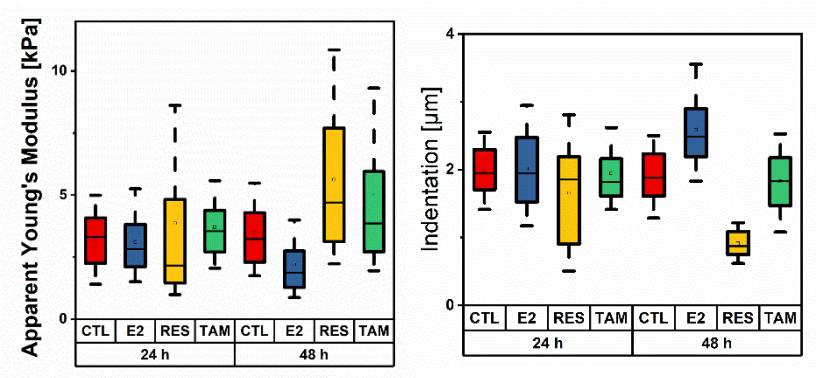

Figure: Apparent Young's Modulus evaluation for cells treated either with estrogen, resveratrol or tamoxifen (Left) and indentation evaluation (right). The box ranges from the 25th to the 75th percentile, while the whisker range from the 10th to the 90th percentile. The mean value is indicated by the black square and the median by the horizontal line inside the box.

New tricks for an old dog: Including afmmulti in the R afmToolkit

Andreas Weber[1], Rafael Benitez[2], José Luis Toca-Herrera[1]

[1]Institute of Biophysics, Department of Nanobiotechnology, University of Natural Resources and Life Science, Vienna, Austria
[2]Department of Business Mathematics, University of Valencia, Spain

Objective

Cells actively respond to external mechanical stresses and show viscoelastic, time- and frequency dependent mechanical properties. One way to probe cell viscoelasticity is to apply step-strains or step-stresses, and then record the change of strain or stress over time (stress relaxation and creep experiment). An interesting thing to consider in this case is that cells are heterogeneous bodies, can actively deform and generate mechanical stress, and show anisotropy of their structure. One therefore has to consider the effect of this anisotropy in determining viscoelastic properties (e.g. probing different cytoskeletal elements at different indentation depths). In addition, viscoelastic show non-linear effects (strain hardening at small strains vs. strain softening at larger ones) and therefore, control and consideration of the strain history is important. Here we introduce time-dependent measurements based on multiple pause segments and present additional functions for the R afmToolkit.

Results & Conclusion

Curves were performed on MCF-7 cells using a pyramidal indenter with a nanometric tips. Then, indentations up to a given force point were performed followed by stress relaxation segments. Naturally, such measurements can be repeated at the same force (meaning indenting up to a force, relaxing, indenting again and so on), different forces, with creep segments or combinations. The figure below shows a Force-distance curve of such a measurement as well as a Force-time and Distance-time curve.

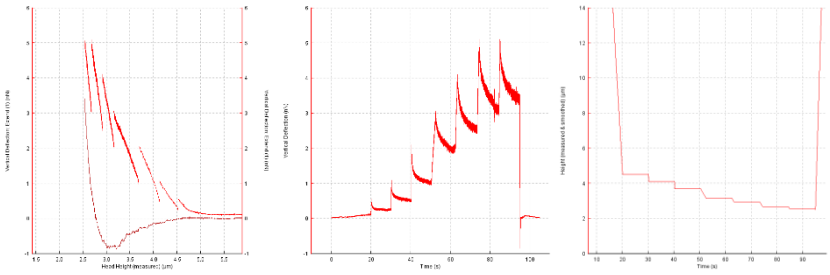

Figure: (Left) Force-distance curve, (Middle) Force-Time curve. (Right) Indentation-time curve of the measurement. The indentation rate was 5 µm/s, the force set-points were 0.5, 1, 2, 3, 4, 5 and 5 nN, with 10 second pause phases.

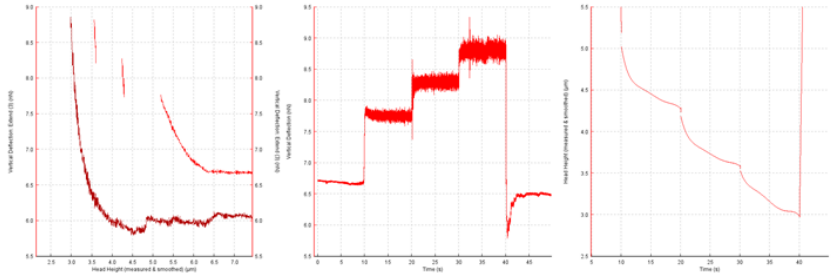

One can easily see that each reaching of the next force setpoint includes a step-wise indentation (see the Figure above, right). Interestingly, the relaxation

behavior appears to change of the given indentation and the respective force. Similarly, multiple creep segments can be done (see below).

The analysis below shows different multiple stress relaxation measurement strategies (4 segments with either rising or constant force, 7 segments with rising forces). In addition, a power law fitting was performed for all curves. This analysis can now be performed automatically in the R afmToolkit.

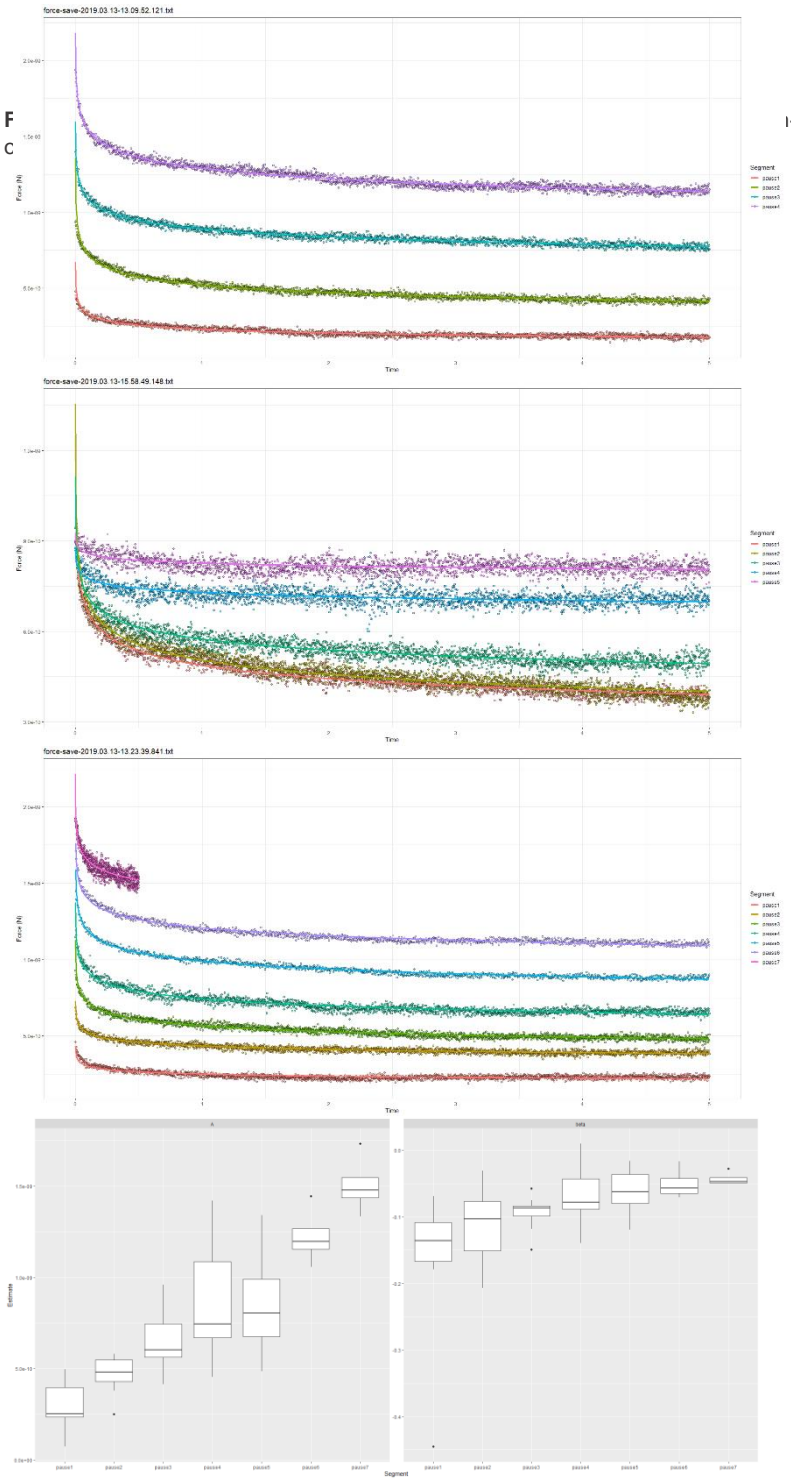

Figure: (Top) Four SR segments at different forces. (Top, 2nd) Four SR segments at same forces. (Third) Seven SR segments at different forces. (Fourth) Statistics of fittings.

3. Publications

SCI articles

1. **A belt for the cell: Cellulosic wall thickenings and their role in morphogenesis of the 3D puzzle cells in walnut shells**
   S.J. Antreich, N. Xiao, JC. Huss, N. Gierlinger
   Experimental Botany 72/13 (2021) 4744
   DOI: 10.1093/jxb/erab197

2. **Unique Reactivity in Surface-Confined Water of Hierarchically Structured Biopolymers**
   M. Beaumont, P. Jusner, N. Gierlinger, AWT. King, A. Potthast, O. Rojaa, T. Rosenau
   Nature communications 12 (2021) 2513
   DOI: 10.1038/s41467-021-22682-3

3. **A guide to elucidate the hidden multicomponent layered structure of plant cuticles by Raman imaging**
   P. Bock, M. Felhofer, K. Mayer, N. Gierlinger
   Frontiers in Plant Science 12 (2021) 1
   DOI: 10.3389/fpls.2021.793330

4. **Raman spectroscopy reveals collagen and phospholipids as major components of hyalinosis in the arteriolosclerotic ulcer of Martorell**
   J. Deinsberger, M. Felhofer, J. Kläger, P. Petzelbauer, N. Gierlinger, B. Weber
   Journal of the European Academy of Dermatology and Venereology 35 (2021) 2308
   DOI: 10.1111/jdv.17573

5. **Raman imaging of Micrasterias: new insights into shape formation**
   M. Felhofer, K. Mayer, U. Lütz-Meindl, N. Gierlinger
   Protoplasma 258 (2021) 1323
   DOI: 10.1007/s00709-021-01685-3

6. **Oak wood drying: precipitation of crystalline ellagic acid leads to discoloration**
   M. Felhofer, P. Bock, N. Xiao, C. Preimesberger, M. Lindemann, C. Hansmann, N. Gierlinger
   Holzforschung 75 (2021) 712
   DOI: 10.1515/hf-2020-0170

7. **Understanding and modelling wildfire regimes: an ecological perspective**
   SP Harrison, IC Prentice, KJ Bloomfield, N Dong, M Forkel, M Forrest, RK Ningthoujam, A Pellegrini, Y Shen, M Baudena, W Cardoso, JC Huss, J Joshi, I Oliveras, JG Pausas, KJ Simpson
   Environmental Research Letters 16 (2021) 125008
   DOI: 10.1088/1748-9326/ac39be

8. **Functional packaging of seeds**
   J.Huss, N. Gierlinger
   New Phytologist 230/6 (2021) 2154
   DOI: 10.1111/nph.17299

9. **A. Cell wall characteristics during sexual reproduction of Mougeotia sp. (Zygnematophyceae) revealed by electron microscopy, glycan microarrays and RAMAN spectroscopy**
   C. Permann, K. Herburger, M. Niedermeier, M. Felhofer, N. Gierlinger, A. Holzinger
   Protoplasma 258 (2021) 1261
   DOI: 10.1007/s00709-021-01659-5

10. **Induction of Conjugation and Zygospore Cell Wall Characteristics in the Alpine Spirogyra mirabilis (Zygnematophyceae, Charophyta): Advantage under Climate Change Scenarios?**
    C. Permann, K. Herburger, M. Felhofer, N. Gierlinger, L. A. Lewis, A. Holzinger
    Plants 10 (2021) 1740
    DOI: 10.3390/plants10081740

11. **Raman imaging reveals in-situ microchemistry of cuticle and epidermis of spruce needles**
    N. Sasani, P. Bock, M. Felhofer and N. Gierlinger
    Plant methods 17 (2021) 1
    DOI: 10.1186/s13007-021-00717-6

12. **Physiological and anatomical responses to drought stress differ between two larch species and their hybrid**
    N. Sasani, LE. Paques, G. Boulanger, A.P. Singh, N. Gierlinger, S. Rosner, O. Brendel
    Trees, 35 (2021) 1467
    DOI: 10.1007/s00468-021-02129-4

13. **Method for high-yield hydrothermal growth of silica shells on nanoparticles**
    M. Willinger, M. Felhofer, E. Reimhult, R. Zirbs
    Materials 14 (2021) 6646
    DOI: 10.3390/ma14216646.

14. **Twist and lock: nutshell structures for high strength and energy absorption**
    N. Xiao, M. Felhofer, SJ. Antreich, JC. Huss, K. Mayer, A. Singh, P. Bock, N. Gierlinger
    Royal Society Open Science 8 (2021) 210399
    DOI: 10.1098/rsos.210399

15. **Measuring biological materials mechanics with atomic force microscopy. 2. Influence of the loading rate and applied force (colloidal particles)**
    A. Weber, B. Zbiral, J. Iturri, R. Benitez, J. L. Toca-Herrera
    Microscopy Research and Technique 84 (2021) 1078
    DOI: 10.1002/jemt.23643

16. **Nanostructured Scaffolds Based on Bioresorbable Polymers and Graphene Oxide Induce the Aligned Migration and Accelerate the Neuronal Differentiation of Neural Stem Cells**
Y. Polo, J. Luzuriaga, J. Iturri, I. Iratorza, J. L. Toca-Herrera, G. Ibarretxe, F. Unda, J.R. Sarasua, J.R. Pineda, A. Larranaga
Nanomedicine 31 (2021) 102314
Doi: 10.1016/j.nano.2020.102314

17. **Cell Stiffness under Small and Large Deformations Measured by Optical Tweezers and Atomic Force Microscopy: Effects of Actin Disruptors CK-869 and Jasplakinolide**
S. Zemljic Jokhadar, J. Iturri, J. L. Toca-Herrera, J. Derganc
Journal of Physics D 54 (2021) 124001
DOI: 10.1088/1361-6463/abd0ae

18. **Nucleotides-Induced Changes in the Mechanical Properties of Living Endothelial Cells and Astrocytes, Analyzed by Atomic Force Microscopy**
J.C. Gil-Redondo, J. Iturri, F. Ortega, R. Pérez-Sen, A. Weber, M.T. Miras-Portugal, J.L. Toca-Herrera, E.G. Delicado
International Journal of Molecular Sciences 22 (2021) 624
DOI: 10.3390/ijms22020624

19. **Encapsulation of opiorphin in polymer coated alginate beads for controlled delivery and pain killing**
S. Stoichev, S. G. Taneva, A. Danailova, J. L. Toca-Herrera, T. Andreeva
Bioautomation 25 (2021) 101
DOI: 10.7546/ijba.2021.25.1.000746

20. **Specific Domain V Reduction of Beta-2-Glycoprotein I Alters Pathogenic Antibody Binding**
I. *Buchholz, T. McDonnell, P. Nestler, S. Tharad, M. Kulke, A. Radziszewska, V. M. Ripoll, F. Schmidt, E. Hammer, J. L.Toca-Herrera, A. Rahman, M. Delcea*
Scientific Reports 11 (2021) 4542
DOI: 10.1038/s41598-021-84021-2

21. **Estrogen Modulates Epithelial Breast Cancer Cell Mechanics and Cell-to-Cell Contacts**
B. Zbiral, A. Weber, J. Iturri, M. dM. Vivanco, J. L. Toca-Herrera
Materials 14 2021 2897
DOI: 10.3390/ma14112897

22. **A New Method for Dispersing Pristine Carbon Nanotubes Using Regularly Arranged S-Layer proteins**
A. Breitwieser, U.B. Sleytr, D. Pum
Nanomaterials 11 (2021) 1346.
DOI: 10.3390/nano11051346

23. **Patterns in Nature - S-Layer Lattices of Bacterial and Archaeal Cells**
D. Pum, A. Breitwieser, U.B. Sleytr
Crystals 11 (2021) 869
DOI: 10.3390/cryst11080869

24. **Crystalline S-Layer Protein Monolayers Induce Water Turbulences on the Nanometer Scale**
R. Tscheliessnig, A. Breitwieser, U.B. Sleytr, D. Pum
Crystals 11 (2021) 1147
DOI: 10.3390/cryst11091147

25. **Workflow for segmentation of Caenorhabditis elegans from fluorescence images for the quantitation of lipids**
T. Lehner, D. Pum, J. Rollinger, B. Kirchweger
Appl. Sci. 11 (2021) 11420
DOI: 10.3390/app112311420

26. **Reaction and diffusion kinetics during hydrothermal carbonization by means of SEM-EDX analysis**
G. Tondl, C. Hammerl, C. Pfeifer, D. Pum
Industrial & Engineering Chemistry Research 59 (2020) 1829
DOI: 10.1021/acs.iecr.9b05643

Other scientific articles

27. **Raman-Mikroskopie an Pflanzen: Neue Einblicke basierend auf Molekülschwingungen**
M. Felhofer, P. Bock, N. Gierlinger
GIT Labor-Fachzeitschrift 65 (2021) 19
https://analyticalscience.wiley.com/do/10.1002/was.0004000124

28. **Raman microscopy on plants: Chemical pictures based on molecular vibrations**
M. Felhofer, P. Bock, N. Gierlinger
Imaging and Microscopy Magazine 23 (2021) 20
https://analyticalscience.wiley.com/do/10.1002/was.0004000131/full/

4. Conferences, seminars, schools and workshops

1. **TITLE: New material based on waste: bacterial cellulose from kombucha production blended with walnut shells**
   AUTHOR: *L. Kaufmann*
   CONFERENCE: ELLS conference Green (r)evolution – from molecules to ecosystems (on-line)
   PLACE: Warsaw (Poland) 2021

2. **TITLE: Walnut shells as ecological substitutes in plastic production**
   AUTHOR: *N. Korp*
   CONFERENCE: ELLS conference: Green (r)evolution – from molecules to ecosystems (on-line)
   PLACE: Warsaw (Poland) 2021

3. **TITLE: How to make a walnut shell: From shell shaping to tissue hardening**
   AUTHOR: *S.J. Antreich*
   CONFERENCE: 23th ATSPB Meeting
   PLACE: Seitenstetten (Austria) 2021

4. **TITLE: A chemical reporter strategy for investigating lignification dynamics in plant cell walls**
   AUTHOR: *O. Morel, S. Hawkins, N. Gierlinger*
   CONFERENCE: 23th ATSPB Meeting
   PLACE: Seitenstetten (Austria) 2021

5. **TITLE: In a nutshell: how cell geometry affects tissue mechanics:**
   AUTHOR: *J.C. Huss*
   CONFERENCE: Ph.D. Program in Biological Sciences
   PLACE: Burapha University (Thailand) 2021

6. **TITLE: Protecting seeds against fire – Lessons from Banksia follicles:**
   AUTHOR: *J.C. Huss*
   CONFERENCE: Online mini workshop on "New Directions in Fire Ecology and Fire Modelling", Imperial College London and King's College London
   PLACE: London (UK) 2021

7. **TITLE: S-layer Protein coated Carbon Nanotubes**
   AUTHOR: *D. Pum, A. Breitwieser, U.B. Sleytr*
   CONFERENCE: MRS 2021 Fall Meeting (on-line)
   PLACE: Boston (US) 2021

8. **TITLE: Nucleotides-induced changes in the mechanical properties of living endothelial cells and astrocytes**
   AUTHOR: *J.C. Gil-Redondo, J. Iturri, F. Ortega, E. Garcia-Delicado, J. L. Toca-Herrera*
   CONFERENCE: 13th Biophysics Congress (EBSA)
   PLACE: Vienna (Austria) 2021

9. **TITLE: Influence of hypoxia on breast cancer cell mechanics (poster with flash talk)**
AUTHOR: *B. Zbiral, A. Weber, M. dM Vivanco, J. L. Toca-Herrera*
CONFERENCE: 13th Biophysics Congress (EBSA)
PLACE: Vienna (Austria) 2021

10. **TITLE: High throughput electric cell characterization**
AUTHOR: *T. Saghaei, A. Weber, E. Reimhult, J.L. Toca-Herrera, P. v. Oostrum*
CONFERENCE: 13th Biophysics Congress (EBSA)
PLACE: Vienna (Austria) 2021

11. **TITLE: Viscoelastic properties of bacteria revisited – an AFM study**
AUTHOR: A*. Weber, R. Benitez, J.L. Toca-Herrera*
CONFERENCE: 13th Biophysics Congress (EBSA)
PLACE: Vienna (Austria) 2021

12. **TITLE: Time- and Zinc-Related Changes in Biomechanical Properties of Human Viscoelastic properties of bacteria revisited – an AFM study** AUTHOR: *J. Iturri, M. Maares, C. Keil, H. Haase, J.L. Toca-Herrera*
CONFERENCE: Cell Physics 2021
PLACE: Saarbrücken (Germany) 2021

13. **TITLE: The more aggressive the softer – comparing the mechanical properties of breast cancer cells**
AUTHOR: *B. Zbiral, A. Weber, M. dM Vivanco, J.L. Toca-Herrera*
CONFERENCE: Cell Physics 2021
PLACE: Saarbrücken (Germany) 2021

14. **TITLE: Viscoelastical properties of MCF-7 cells modulated by substrate stiffness**
AUTHOR: *J.C. Gil-Redondo, A.Weber, B. Zbiral, Maria dM. Vivanco, J.L. Toca-Herrera*
CONFERENCE: Cell Physics 2021
PLACE: Saarbrücken (Germany) 2021

15. **TITLE: A-to-I RNA editing of Filamin A (FLNA) regulates cellular adhesion, migration and mechanical properties**
AUTHOR: *A. Weber, M. Jain, G. Manjaly, J. Deek, M. Stulic, A. Bausch, M. F. Jantsch, J. L. Toca-Herrera*
CONFERENCE: Cell Physics 2021
PLACE: Vienna (Austria) 2021

16. **TITLE: Power law rheology to describe cell mechanics**
AUTHOR: *A. Weber, B. Zbiral, R. Benitez, M.dM. VIvanco, J. L. Toca-Herrera*
CONFERENCE: 26th Congress of the ESB (ESBiomech2021)
PLACE: Milano (Italy) 2021

17. **TITLE: Tamoxifen resistance leads to softening of breast cancer cells** AUTHOR: *B. Zbiral, A. Weber, M.dM. VIvanco, J. L. Toca-Herrera*
CONFERENCE: 26th Congress of the ESB (ESBiomech2021)
PLACE: Milano (Italy) 2021

18. **TITLE: Hypoxic conditions alter breast cancer cell mechanics and rheology**
AUTHOR: *B. Zbiral, A. Weber, M.dM. VIvanco, J. L. Toca-Herrera*
CONFERENCE: 12th Annual Symposium Physics of Cancer
PLACE: Leipzig (Germany) 2021

19. **TITLE: Modulation of viscoelastic properties of MCF-7 cells by substrate stiffness**
AUTHOR: *J.C: Gil-Redondo, A.Weber, B. Zbiral, M.dM. VIvanco, J. L. Toca-Herrera*
CONFERENCE: 12th Annual Symposium Physics of Cancer
PLACE: Leipzig (Germany) 2021

20. **TITLE: Mechanical properties of biomimetic protein filme by using AFM**
AUTHOR: *M. Sumarokova, A. Weber, J. Iturri, J. L. Toca-Herrera*
CONFERENCE: The 6th International Symposium and Schools for Young Scientists on Physics, Engineering and Technologies for Biomedicine
PLACE: Moscow (Russia) 2021

5. Ongoing projects, national and international collaborations

Projects (and research)

https://boku.ac.at/nano/biophysics/forschung

Main collaborations

- **Prof. Peter Lieberzeit**, Univ. of Vienna, Inst. of Anal. Chem., Vienna, Austria
- **Prof. Carole C. Perry**, Nottingham Trent University, Nottingham, UK
- **Dr. Rafael Benítez**, Univ. of Extremadura, Dept. of Mathematics, Spain
- **Dr. Luis Millán González**, Univ. of Valencia, Dept. of Physical Education and Sport, Spain
- **Dr. Chartchai Krittanai**, Mahidol University, Institute of Molecular Biosciences, Thailand
- **Prof. M. Schneider**, Institute biopharmacy and pharmaceutical technology, University of Saarland
- **Prof. Georg Papastavrou**, Faculty of Biology, Chemistry, and Earth Sciences, University of Bayreuth, Germany
- **Dr. Maria Vivanco**, CICbioGUNE, Spain • Prof. Longjian Xue, Wuhan University, China
- **Dr. Felipe Ortega**, Universidad Complutense, Madrid, Spain • Prof. Ronald F. Ziolo, CIQA – Conacyt, Mexico
- **Dr. Spela Zemlijc**. University of Ljubljana, Slovenia • Prof. Hajo Haase / Dr. Claudia Keil, TU-Berlin, Germany
- **Dr. Anders Lundgren**, Chalmers University, Sweden • Prof. Ingo Burgert, ETH Zurich, Switzerland
- **Dr. Michaela Eder**, Max Planck Institute of Colloids and Interfaces, Potsdam, Germany
- **Prof. Anna de Juan**, Chemometrics group, University of Barcelona, Diagonal 645, 08028 Barcelona, Spain
- **Yaseen Mottiar, Prof. Shawn D Mansfield**, University of British Columbia, Forest Sciences Centre, Vancouver, Canada
- **Prof. Gilbert Neuner**, University of Innsbruck, Institute of Botany, Unit Functional Plant Biology, Innsbruck, Austria
- **A.o. Univ. Prof. Ursula Lütz-Meindl**, University of Salzburg, Cell Biology and Physiology Department, Salzburg, Austria
- **Prof. Wolfgang Gindl**, Institute for Wood technology and Renewable materials, University of Natural Resources and Life Sciences, Vienna, Austria